Received: 27 November 2023 | Revised: 4 March 2024 | Accepted: 20 April 2024

DOI: 10.1002/eqe.4142

RESEARCH ARTICLE

WILEY

Applicability of 1D site response analysis to shallow sedimentary basins: A critical evaluation through physics-based 3D ground motion simulations

Junfei Huang[1] | **David McCallen**[2]

[1]Department of Civil and Environmental Engineering, University of Nevada, Reno, Nevada, USA

[2]Energy Geosciences Division, Lawrence Berkeley National Laboratory, Berkeley, California, USA

Correspondence
David McCallen, Critical Infrastructure Program, Energy Geosciences Division, Lawrence Berkeley National Laboratory, Berkeley, California, USA.
Email: dbmccallen@lbl.gov

Funding information
U.S. Department of Energy Exascale Computing Project, Grant/Award Number: 17-SC-20-SC; U.S. Department of Energy Nuclear Safety Research and Development Program

Abstract

One-dimensional site response analysis (1D SRA) remains the standard practice in considering the effect of local soil deposits and predicting site-specific ground motions, although its range of applicability to realistic seismic wavefields is still in question. In this 1D approach, horizontal and vertical ground shaking are assumed to be induced by vertically propagating shear and compressional waves, respectively. A recent study based on analytical two-dimensional (2D) plane waves and simple point source earthquake simulations has shown two mechanistic limitations in this 1D modelling technique for general inclined seismic waves, that is, systematic over-prediction of the vertical motion and wave trapping in the 1D soil column. In this article, we evaluate in detail the applicability of this 1D modelling approach to realistic three-dimensional (3D) simulated seismic wavefields in shallow sedimentary basins. Linear-viscoelastic 1D SRA predictions using two types of input motions that are commonly used in practice—rock outcrop and in-column motions, are compared with the reference true site response results from 3D earthquake simulations in terms of various measures in the frequency and time domain. It is shown that the horizontal motion in the 3D seismic wavefield exhibits dominant shear wave propagation phenomenon, while the vertical motion is a combined effect of compressional and shear waves and can be over-predicted by the 1D approach when the incident seismic waves are inclined. Direct evidence of the wave refraction process that leads to the vertical motion over-prediction is provided. 1D SRA with in-column inputs can yield motions that have significantly longer duration compared to the true 3D site response solution due to trapped waves, casting in doubt the frequent need for increased soil damping in existing site studies to compensate for wave attenuation due to scattering alone. Sensitivity investigation on the increase of soil profile damping by a multiplier D_{mul} shows D_{mul} values compatible with those found in the literature for both horizontal and vertical motions. It is shown

that the level of D_{mul} optimized for a best match of the spectral acceleration is dependent on the characteristic of the input motion and a larger D_{mul} is typically required for the vertical component. In contrast, 1D SRA with outcrop motions predicts motions with shorter significant duration due to its inability to capture the basin-edge generated surface waves. A suite of ground motion simulations was performed to assess the sensitivity of the observations to the basin geologic structure including the velocity gradient, rock-basin impedance contrast and basin depth. The analysis results show that the accuracy of the simplified 1D procedure is dependent on the wavefield composition of both the input motions and the true 3D site response solution. While the horizontal motions in shallow sedimentary basins can, to the first order, be reasonably captured by the simplified 1D approach, 1D SRA for the vertical component is in general not reliable and contributions from inclined shear waves should be accounted for in site-specific evaluation of the vertical design ground motion.

KEYWORDS
1D assumption, 3D ground motion simulation, inclined seismic wave, site response analysis, vertical ground motion, wave propagation

1 | INTRODUCTION

It is well recognized that seismic waves will be modified by the local surficial soil sediments when approaching the ground surface, resulting in ground motions with amplitude, duration, and frequency content that can differ significantly from the incoming wavefield. Evaluation of these modifications, commonly known as the local site effects, is an integral part of seismic hazard evaluation and calculation of site-specific ground motions. To model the complex response of soil deposits during earthquake shaking, one-dimensional site response analysis (1D SRA) is widely used in engineering applications. This approach assumes that the seismic waves reaching the site are nearly vertically propagating due to wave refraction through the upper crustal velocity gradient and the local soil is composed of stacked horizontal layers without lateral heterogeneity. These assumptions, which were introduced during the pioneering works in the 1950s–1970s[1–3] and are collectively referred to as the "1D assumption" in this article, are now broadly adopted in various aspects of earthquake engineering, for example, seismic hazard calculation,[4] site response calibration,[5] and soil-structure interaction,[6] among others.

Although 1D SRA is the dominant method in evaluating the local site effects, it has many known limitations due to its simplified 1D approach in simulating the complex wavefield incurred by real earthquakes. Apart from the effects of impedance contrast and soil nonlinearity that it partially models, the true site response is also influenced by important 2D and 3D effects including inclined seismic waves and their mode conversion, basin and topography, lateral heterogeneity, and soil multi-axial constitutive behavior.[7,8] These limitations, combined with the uncertainties in site characterization of subsurface soil properties and input motion for the soil column,[9–11] often result in considerable disagreement between observations and 1D SRA predictions.[9,12–15] With the increasing number of available records in downhole seismic arrays deployed worldwide, in recent years, studies have tried to assess the validity of 1D SRA and identify the different levels of complexity in simulating the local site response. For instance, Thompson et al.[9] concluded that only 16 sites out of the selected 104 downhole arrays in the KiK-net strong-motion network in Japan demonstrated one-dimensional site response based on low inter-event variability and good fit to the theoretical 1D transfer function. Pilz and Cotton[14] examined 354 KiK-net sites and found 45% of these selected sites were influenced by 2D and 3D effects. In a recent taxonomy study, Tao and Rathje[15] examined 34 sites in Japan and the United States and 69% of the sites were considered suitable for 1D analysis. While the employed criteria and datasets are different in certain aspects, these studies clearly show that deviation of real-world site response from the 1D assumption is common.

Deficiency in the existing 1D SRA approach is especially of concern for vertical ground motion assessment. In earthquake engineering, focus has traditionally been on the horizontal ground motions due to their large amplitude as well as

the observed structural damage patterns attributed to lateral forces, while the vertical components are largely disregarded and relevant studies are lagging behind. Notably, all the aforementioned investigations on the performance of 1D SRA are for the horizontal motions only. However, vertical motions well exceeding 1 g and larger than their horizontal counterparts have been repeatedly recorded in recent earthquakes, prime examples including the 4 g record in the 2008 Mw 6.9 Iwate-Miyagi Nairiku earthquake in Japan,[16] and peak vertical-to-horizontal acceleration ratios up to 4.8 in the 2011 Mw 6.3 Christchurch earthquake in New Zealand.[17] Field and experimental evidence of structural and non-structural failures in buildings and bridges caused by severe vertical motions were also documented and recognized.[18,19] In view of the potential damaging effects, renewed interest in properly characterizing the vertical motions has been growing. Historically, the "2/3 V/H rule[20]" by which the vertical response spectrum is roughly estimated as two-thirds of the corresponding horizontal component, is used in many design guidelines worldwide. It was not until recently in 2016, the ASCE/SEI 7 standard,[21] one of the key documents for building design in the United States, updated the specification on vertical ground motion assessment based on recent studies of V/H ratios to reflect the important frequency-dependent relationship between the vertical and horizontal motions. This is considered an expedient approach, however, not only because of the practical limitations in the empirical V/H ratios to represent attenuation relations that may differ from the horizontal component, resulting in additional uncertainties,[22] but also the difficulty in applying it to site-specific ground motion procedures and soil-structure interaction analysis that are required for critical infrastructures.[23] To obtain site-specific ground motions, 1D SRA is typically performed in current practice. Following the 1D assumption, horizontal and vertical motions are assumed to be decoupled and are induced by vertically propagating shear and compressional waves, respectively.[3,19,21] However, in contrast to horizontal motions which are reported to be predicted with reasonable confidence,[24] vertical motions predicted using the simplified 1D assumption are observed to be inconsistent with field observations. Based on the 1D vertical P wave propagation model, Elgamal and He[19] found that approximately 25% reduction in the P wave velocity and unphysically high damping (15%–25%, even for small tremors) were needed to obtain a good match with the recorded vertical response at the Lotung downhole array in Taiwan, in agreement with findings by Mok et al.[25] Tsai and Liu[26] employed a similar optimization procedure on five downhole array profiles to calibrate the vertical response on a site-to-site basis, resulting in different levels of velocity reduction and damping increase. In soil-structure interaction analysis, the 1D assumption on vertical P wave propagation has caused anomalously high site amplification and spatial coherency in the vertical direction, which have led to overly conservative structural and equipment designs.[23,27] As a result, 1D vertical P wave propagation is considered unreliable and seldom used in current practice.[6,23,24,27] The performance of 1D vertical SRA becomes more perplexing considering that few successful applications of this approach for vertical response modelling are found in the literature, for example, the works by Johnson and Silva,[28] Fujii et al.,[29] and Yang and Yan.[30] This indicates that the amplification mechanism for the vertical motion may be fundamentally different from that of vertically propagating compressional waves, and the prediction accuracy can be dependent on the subsurface condition and characteristics of the incoming wavefields consisting of both P and SV waves. Seismic waves incurred by real earthquakes are rarely vertically propagating, and observations indicate that the incident angle of seismic waves can be large due to the complex wave focusing and scattering phenomena. Considering the large amplitude of S waves, even a small incident angle can lead to significant vertical components and result in seismic response of structural systems substantially different from that based on simplified modelling approaches.[31,32] Silva[33] showed that for generic rock and soil sites, the high-amplitude part of vertical motions can be in phase or out of phase with that of the horizontal motions depending on SV wave refraction at the base of the profile and distance of the site from the source. Based on spectral ratios calculated between the P and S wave windows, Beresnev et al.[34] concluded that the vertical motion is dominated by SV waves below about 10 Hz, above which the contribution from P waves is about as strong or greater. The influence of inclined SV waves on the vertical motion is also confirmed by the strong S-to-P conversion observed in downhole array studies.[35,36] Particularly, Chao et al.[37] compiled the P- and S-wave arrival times of 37,888 strong vertical motion records from both crustal and subduction earthquakes in Taiwan and reported that approximately 73% of the recordings are classified as S-dominated, that is, the peak vertical acceleration and spectral response occurs within the S wave window, suggesting the strong correlation between the vertical site amplification and S waves.

In a recent study based on analytical 2D plane waves and simple point source earthquake simulations, Huang and McCallen[38] identified two deficiencies inherent in the 1D modelling approach, namely, the systematic over-prediction of the vertical motion due to its inability to capture the refraction process of inclined shear waves, and the excessively long-duration motions predicted with the in-column input motion incurred by the enforced fixed boundary at the 1D soil column base that is unable to accommodate the outgoing waves leading to trapped energy and spurious resonance, especially in the vertical direction. However, unlike the idealized 2D and 3D waves with well-separated wave phases, realistic seismic waves from an extended earthquake source are complicated by the simultaneous contribution of various

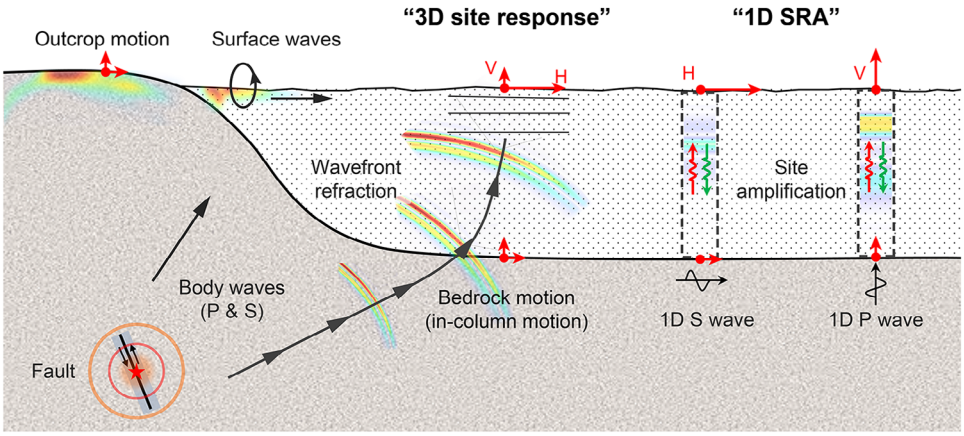

FIGURE 1 Inclined body wave refraction and surface wave propagation in the sedimentary basin in true 3D site response compared with the surface motion predictions by 1D SRA for the horizontal and vertical components. The colour shading in the figure shows consecutive wavefront snapshots of the simulated 3D wavefield from a point source earthquake simulation and the corresponding 1D wavefields by the 1D approximation.

wave types (i.e., P, S and surface waves), and the wavefield composition is expected to vary spatially owing to the difference in the wave attenuation rate and complex wave interferences. Considering the physical nature of the identified mechanistic limitations, the 1D accuracy and potential bias for both the horizontal and vertical site response predictions are likely dependent on the characteristics of the 3D wavefields and the associated geological structure, which remains unclear and requires further investigation.

In view of the major strides in high-performance computing and earthquake modelling,[39–41] broadband fully deterministic 3D ground motion simulation is becoming an appealing alternative to the engineering community. Complex seismic wave propagation in 3D heterogeneous geological structures across a broad frequency band can be captured through this deterministic approach.[42] In contrast to the continuing limited ground motion recordings from real earthquakes, spatially dense ground motions can be simulated at any location within the regional-scale computational domain.[43] Since the geological structure employed in the simulation is fully known, this approach provides a unique opportunity to evaluate the applicability of the 1D approximation technique while avoiding the uncertainties in subsurface characterization and input motion selection that are commonly observed in existing field site response investigations. In this article, based on high-fidelity physics-based ground motion simulations, we perform extensive evaluation of the applicability of 1D SRA for both the horizontal and vertical motions when applied to realistic 3D seismic wavefields. In the remaining sections, we first briefly introduce the two mechanistic limitations identified in the 1D approximation process and present the characteristics of the simulated ground motion datasets for canonical basin models that are representative for shallow crustal earthquakes. We then report the performance of 1D SRA through detailed frequency- and time-domain comparisons between the 1D SRA predictions and the reference 3D ground motions. Discrepancies in the amplification mechanism of the horizontal and vertical site response are illustrated, and the spatial variability of the accuracy of the 1D approach is explained in terms of the wavefield composition of both the input motions for 1D SRA and the reference true 3D solutions. The sensitivity of these observations to the geologic profile of the sediments is further demonstrated. The article aims to emphasize the difference in the characteristics of the horizontal and vertical site response, the contributing factors to the accuracy of the 1D modelling approach, and important implications for site-specific design ground motion assessment.

2 | BRIEF SUMMARY OF THE IDENTIFIED LIMITATIONS IN 1D SRA

2.1 | Implications of the 1D assumption for inclined body waves

The ground shaking at an engineering site in a sedimentary basin, as is the case in many metropolitan areas, is caused by body waves from the rupturing fault and later-arriving surface waves, as illustrated in Figure 1. In 1D SRA, it is assumed that the severe shaking portion of the ground motion is dominated by the body waves, and the seismic waves reaching the site are nearly vertically propagating due to the upper crustal velocity gradient and the local soil is composed of nearly

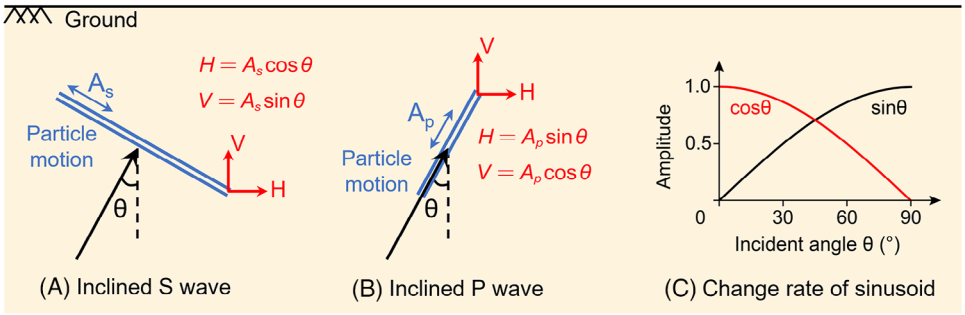

FIGURE 2 Horizontal and vertical components of inclined S (with amplitude A_s) and P (with amplitude A_p) waves and their sensitivity with the incident angle θ.

horizontally stacked layers without lateral heterogeneity. However, seismic waves are rarely perfectly vertically propagating when arriving at the site under consideration. When inclined seismic waves impinge on the surficial soft layers, the incident shear and compressional waves will undergo an additional refraction process when propagating through the soft sediments. For shear waves, this leads to a gradually increasing horizontal component and a decreasing vertical component; for compressional waves, the reverse would be observed, which leads to a gradually decreasing horizontal component and an increasing vertical component. When performing 1D SRA to approximate the 3D site response due to inclined body waves, it was demonstrated in Huang and McCallen[38] that 1D SRA can lead to significant vertical motion over-prediction as the vertical input motions are obtained when the inclined shear waves have a relatively large vertical component while the 1D approach not only fails to capture the diminishment of this component occurring in the later shear wave refraction process, but also further amplifies the input motions through the classical 1D site amplification mechanism. The same physical interpretation also applies to the prediction of horizontal motions, that is, 1D SRA using horizontal input motions that partly come from inclined P waves may, in a similar manner, lead to over-prediction of the horizontal motions.

Following the same physical argument, an accompanying effect of this shear and compressional wave refraction process is that 1D SRA will tend to under-predict the horizontal component of inclined S waves and the vertical component of inclined P waves at large incident angles. Figure 2 shows schematically the horizontal and vertical components of the inclined S and P waves and their change rate with the incident angle θ. As can be seen, the vertical component of S waves and the horizontal component of P waves are associated with $sin\theta$ while the remaining other component is associated with $cos\theta$. This indicates that although the horizontal component of S waves and the vertical component of P waves are not sensitive to small incident angles, they will have a relatively large deduction when θ becomes large, so will be the input motions for 1D SRA. The corresponding 1D predictions are prone to be smaller than the 3D site response solutions due to the refraction-induced increase of the respective components. As a result, for the inclined body wave approximation, there are two competing factors that may influence the prediction bias of the 1D modelling procedure, and the result will be dependent on the actual wave composition at the site. As mentioned earlier, the body wave portion of realistic seismic wavefields is a combination of P and S waves. Although direct P waves are usually considered of much smaller amplitude compared to shear waves (by the ratio of 1/5 for a Poisson solid[33]) and may only have secondary effects, converted P waves from direct S waves may be substantially larger and contribute non-negligibly to the incident wavefield especially at large distances due to the lower P wave attenuation compared to that of the S waves. The extent to which the two competing factors will manifest themselves in the 1D predictions of the horizontal and vertical motions remains to be better understood.

2.2 | Wave trapping in the 1D soil column

It is shown in previous site response studies that 1D SRA often predicts the so-called spurious resonance, that is, high levels of amplification near the vibration periods of the 1D soil column that are not observed in field records, with resonant frequencies typically shifted towards lower frequencies compared to that calculated with the field data. This phenomenon is postulated to be caused by the idealization of perfect horizontal layering of the soil deposit, and exclusion of soil nonlinearity and wave scattering.[44,45] It is argued that the constructive and destructive wave interference would not develop

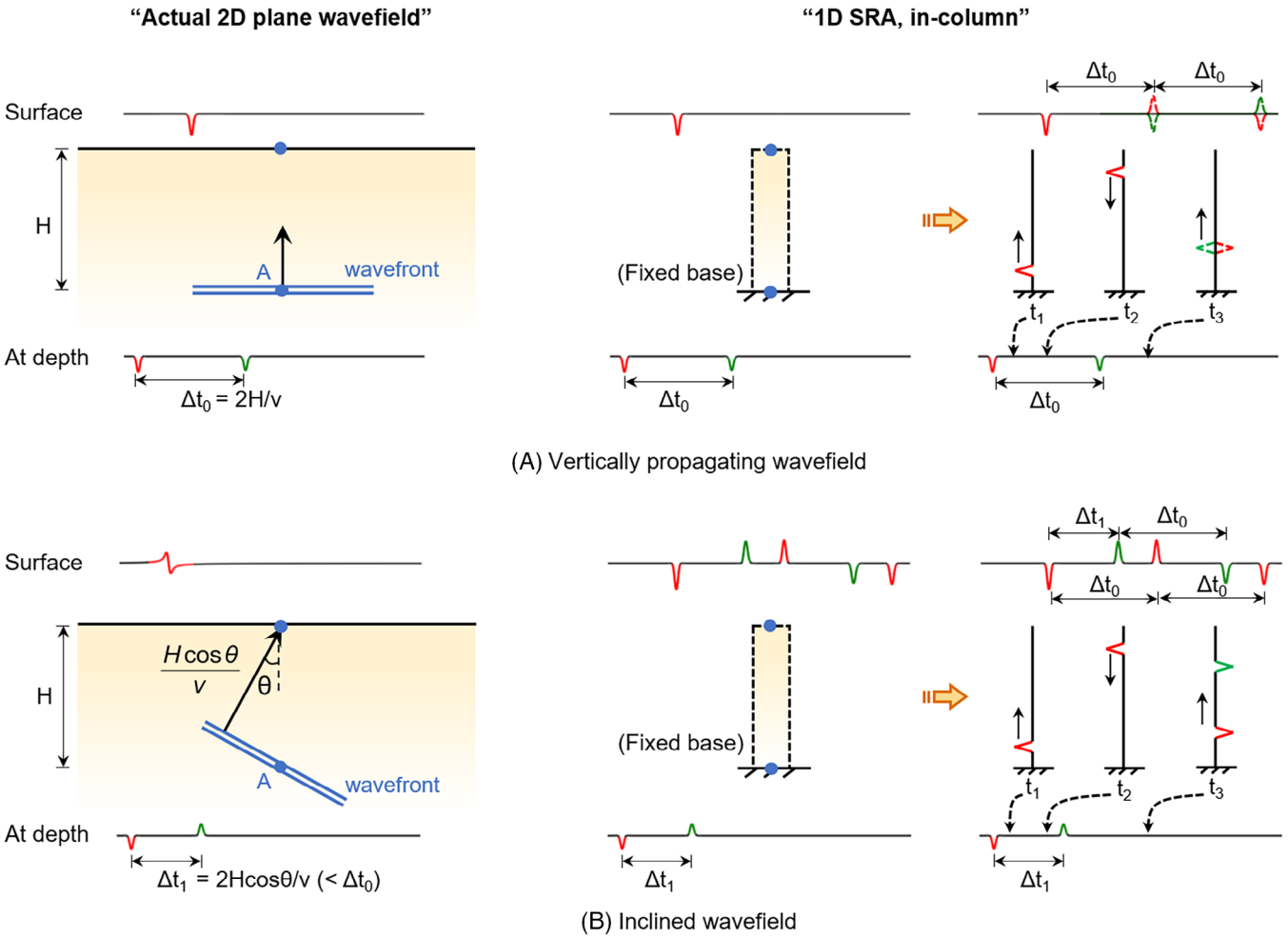

FIGURE 3 1D SRA with the in-column input motion when approximating a vertically propagating wavefield (A) and inclined wavefield (B) in a homogeneous half-space. In each panel, the actual 2D wavefield and the corresponding 1D SRA results are illustrated along with the motions at the surface and at depth. Snapshots of the propagating waves in the 1D column at three instants in time (t_1, t_2 and t_3) are shown to demonstrate the polarity of the upgoing and downgoing waves and difference in the wave interference of the two cases. For clarity, wave mode conversion is not considered in the 2D solution and time-synced movies of the travelling wave pulses in the two cases can be found online in the Material S1 (Figure S3A.mp4) and S2 (Figure S3B.mp4).

in the field due to lateral heterogeneities in the velocity structure and nonlinear soil response. However, it is unlikely that wave scattering and soil nonlinearity alone would explain the large amplification near the site periods, as this is also observed in relatively well-characterized soil profiles with small lateral velocity changes and under the excitation of weak motions (i.e., essentially linear behaviour).[45–47] We speculate that this phenomenon may have strong correlation with the limitation in the simplified 1D modelling method for inclined seismic waves that have led to complex wave interferences of trapped waves in the 1D soil column vibrating near the site periods for an excessively long time.[38]

For demonstration purposes, we show in Figure 3 the 1D approximation results of two different 2D plane wavefield cases in a homogeneous half-space with wave velocity v, and a reference point A that records the 1D in-column input motions at depth H. In both Figure 3A and B, the actual 2D wavefield is shown on the left-hand side, with the upgoing incident and downgoing reflected waves denoted by the red and green pulses, respectively; the 1D soil column employed in 1D SRA with the in-column input motion is shown on the right-hand side, with the colour coding of the wave pulses corresponding to the resultant waves incurred by the respective red and green pulses from the actual 2D wavefield on the left. For clarity, converted waves is not considered in the 2D solution and time-synced movies of the travelling wave pulses in the two cases can be found online in the Material S1 (Figure S3A.mp4) and S2 (Figure S3B.mp4). For vertically propagating waves (Figure 3A), the surface motion shows a single pulse corresponding to the arrival of the incident wave at the surface, while the motion at depth displays two pulses corresponding to the incident and reflected waves with a time

separation $\Delta t_0 = 2H/v$. When performing 1D SRA to approximate the local site response, the total recorded motion at point A is used as the in-column input motion, and without a priori information, both wave pulses would serve as equivalent forces that excite the soil column with the only difference being the timing of the excitation. It turns out 1D SRA in this case predicts the exact same results as the actual 2D wavefield, as expected. A detailed inspection of the snapshots of the propagating waves in the fixed-base 1D column reveals that the reflected upgoing wave from the base (red dashed pulse at t_3) introduced by the first incident wave pulse from the actual wavefield is in exact opposite waveform with the upgoing wave (green dashed pulse at t_3) introduced by the second reflected wave pulse from the actual wavefield at the exact same time, resulting in full cancellation of the later propagating waves in the 1D column. In other words, the fixed boundary at the base is transparent to the outgoing wave reflected from the surface and this ensures the correct solution for the actual 2D wavefield. In Figure 3B, the actual 2D site response is induced by inclined incident and reflected waves propagating horizontally by the site, with the incident wave first arriving at point A below the site of interest and the reflected wave then leaving point A within time $\Delta t_1 = 2Hcos\theta/v$, smaller than the time separation Δt_0 in the case of vertically propagating waves given the fact that the inclined wave travel path from point A to the surface is effectively shorter than the full vertical depth of the soil column. In the 1D modelling of this inclined wavefield, the total recorded motion at A would again be used as the in-column input motion. However, since the waves are still assumed to be vertically propagating in the soil column, the upgoing wave (green pulse at t_3) introduced by the reflected wave from the actual inclined wavefield will depart from the column base earlier than the reflected upgoing wave (red pulse at t_3) incurred by the first incident wave from the actual inclined wavefield. Since the boundary becomes silent afterwards, the two upgoing waves shown at t_3 will then always undergo total reflection at the base and get trapped in the soil column near the site periods, leading to predicted wave trains with excessively long duration. As can be seen, the wave phase in the in-column input motion that corresponds to the outgoing reflected wave in the actual inclined wavefield has served as effectively an extra input source for the 1D column. Therefore, the observed multiple reverberations are a combined effect of trapped outgoing waves and resulting spurious excitation at the base in the later phases. It is noted that this phenomenon will be more prominent in the vertical direction because of the difference in the assumed wave speed (i.e., P wave speed instead of the S wave speed will be used if the S wave contribution to the vertical motion is indeed large) and wave attenuation rate that can lead to more complex wave interferences in the 1D column. For inhomogeneous soil layers (i.e., soil properties vary with depth), this phenomenon is expected to be more significant and occurs even when using the outcrop input motion, as the downgoing waves will undergo multiple reflections before escaping into the underlying half-space.

In view of the large amplification near the site periods, in existing site response studies, researchers have often tried to optimize the soil damping profile to achieve a best match scenario with the recorded data,[9,13,19,26,46,47] typically resulting in increased damping levels compared to the small-strain damping profile determined based on laboratory measurements, even for small tremors. It should be noted that although this optimization process may be useful in improving the 1D predictions empirically on a site-to-site basis, it does not necessarily provide persuasive physical basis on the soil profile change and may have undesirably extended the range where the 1D approach is considered applicable. Based on physics-based earthquake simulations, one purpose of this study is to, in a deterministic manner, investigate the characteristics and implications of the trapped waves incurred by the 1D modelling method, and the efficacy of increased soil damping in the improvement of the 1D SRA results.

3 | SIMULATED GROUND MOTION DATASET

3.1 | Physics-based 3D ground motion simulations

In this study, spatially dense high-fidelity ground motions from physics-based 3D earthquake simulations are utilized as input motions and reference true 3D site response solutions to evaluate the validity of 1D SRA for realistic complex seismic wavefields. Since we are interested in understanding the mechanistic difference between 3D site response and its 1D approximation in terms of wave propagation physics, instead of relying on stochastic simulation methods or empirical ground motion models (GMMs) that are approximate and statistical, we employed this fully deterministic earthquake simulation approach to solve the governing elastodynamic wave equations explicitly across a broad frequency range such that the site-to-site ground motion variations due to 3D wave propagation can be captured.[42] The earthquake simulations were performed using SW4 (Seismic Waves, 4th order), an efficient and verified time-domain fourth-order accurate finite difference program developed for simulating anelastic seismic wave propagation on massively parallel computers.[48] SW4 is a key component in the recently developed EQSIM fault-to-structure computational framework[39,49] and has many

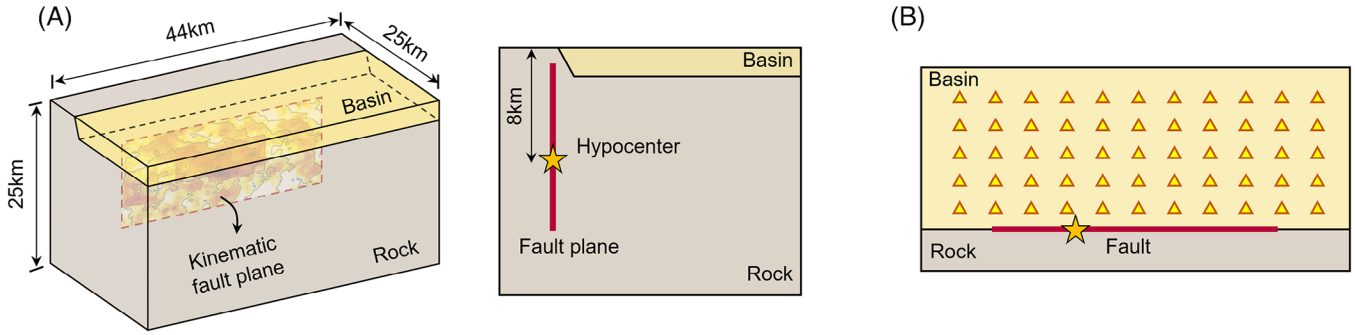

FIGURE 4 Physics-based 3D ground motion simulation for the Mw 6.5 strike-slip event: (A) perspective and side views of the canonical basin model; (B) recorded sites on a 500 m×500 m grid in the sedimentary basin.

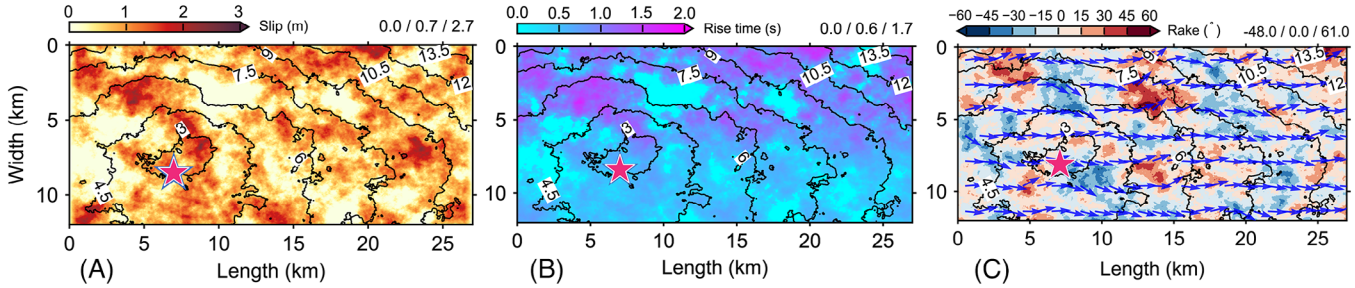

FIGURE 5 Grave-Pitarka kinematic rupture model for the simulated Mw 6.5 strike-slip event: (A) slip; (B) rise time; and (C) rake angle. In each panel, the hypocentre is denoted by the red star; the rupture fronts (black contour lines) are at 1.5-s intervals; the top right corner shows the minimum, median and maximum values of the respective rupture properties; the slip directions (blue arrows) are shown along with the colour shading.

desirable 3D seismic modelling capabilities, including the built-in curvilinear and cartesian mesh generators, far-field absorbing super-grid boundaries, anelastic attenuation for P and S waves, and support for surface topography and fully 3D heterogeneous material model representation. Since doubling the maximum resolved frequency in 3D simulations requires 16 times greater computational effort, our ground motions are solved between 0 and 5 Hz with at least eight points per shortest wavelength. Given the significant computational efforts, the numerical simulations described herein were conducted on Perlmutter, a GPU-accelerated high-performance computing platform at the National Energy Resources Scientific Computing Center (NERSC).[50]

Since we are not intending to model the ground motions of a historical earthquake event which will require an event-specific fault rupture realization and velocity structure, we consider 3D seismic wave propagation in regional-scale canonical basin models induced by a representative Mw 6.5 strike-slip earthquake scenario, as shown in Figure 4. The canonical basin model encompasses a flat-surface region of 44 km × 25 km spanning in the horizontal directions and 25 km in the vertical direction, with a shallow sedimentary basin alongside a 1D layered crust and a vertical fault rupture plane placed near the basin edge. This regional model was created to be representative of the geologic environment of common shallow crustal earthquakes while intended to be simple enough to allow for parametric exploration of the basin amplification effects in the near field, which are of high engineering interest. The rectangular fault rupture plane is determined to be 27 km × 12 km based on empirical relations between seismic moment and fault area for strike-slip events, and the hypocentre is located near the quarter point of the fault length direction and at a depth of 8 km. In the SW4 simulations, the rupturing fault is explicitly modelled as spatially distributed point sources with the complex rupture characteristics, including the spatially correlated depth-dependent slip, rise time and rake angle distribution prescribed by the Grave-Pitarka kinematic rupture model,[51,52] as shown in Figure 5. This kinematic rupture modelling technique has been successfully used in both validation studies for many historical earthquakes and predictive simulations of potential large earthquake scenarios. Further details about the rupture model used in this research work are described in Pitarka et al.[52] and the references therein.

Due to the depositional nature of soil deposits, detailed in situ investigation of site soil profiles typically shows depth-dependent soil properties, and generic velocity profiles developed for basin sediments often have the regression form of a

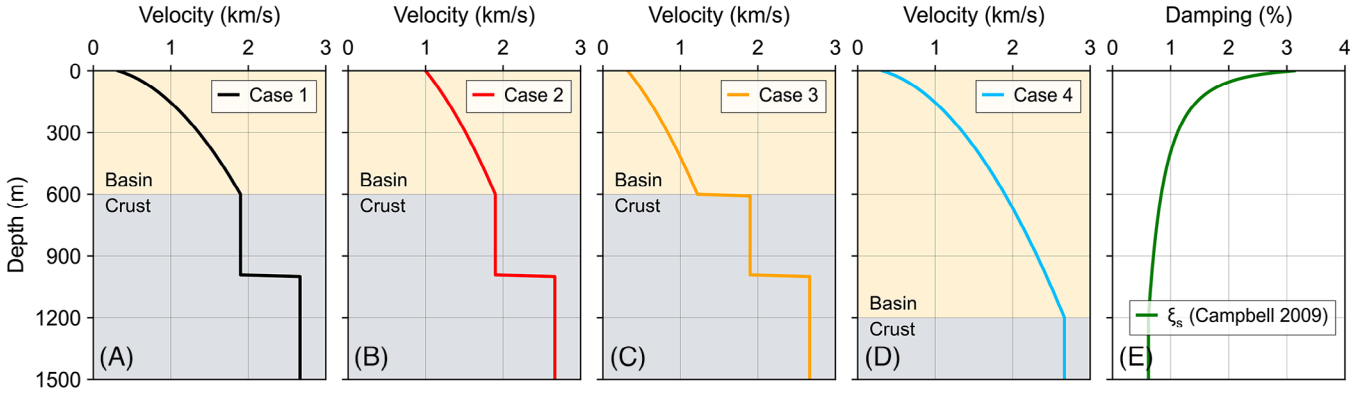

FIGURE 6 Shear wave velocity and damping profiles for the sedimentary basin considered in the parametric study: (A) case 1 (baseline case); (B) case 2 (velocity gradient); (C) case 3 (impedance contrast); (D) case 4 (basin depth); (E) shear wave damping.

power-law function. In this study, we consider the shear wave velocity of the sedimentary basin to follow the generalized power law function below[53]

$$V_s(z) = V_H\left[b + (1-b)\frac{z}{H}\right]^n \tag{1}$$

where b is defined as a function of the shear wave velocity at the surface (V_0) and base (V_H) of the soil profile (i.e., $b = (V_0/V_H)^{1/n}$), H is the basin depth, n is a dimensionless inhomogeneity factor varying in the common range of 0 to 1, and z is the depth measured from the surface. To investigate the influence of basin geological structure on the accuracy of 1D SRA, we consider four basin profile cases, as shown in Figure 6. Case 1 serves as our baseline case with $V_0 = 320$ m/s, $V_H = 1900$ m/s, $H = 600$ m. Compared to case 1, case 2 has $V_0 = 1000$ m/s, which results in a basin profile with smaller velocity gradient; case 3 has $V_H = 1220$ m/s, which leads to a sharp velocity contrast (~1.56) at the base of the basin; case 4 follows the same power-law function as in case 1 except z is extended to a larger basin depth value $H = 1200$ m. For simplicity, all cases have a linear density profile varying from 2140 kg/m^3 at the surface to 2450 kg/m^3 at the base of the basin, and use the same depth-dependent shear wave quality factor Q_s determined as follows[54] (Figure 6E):

$$Q_s = \frac{1}{2\xi_s} = 7.17 + 0.0276V_s \tag{2}$$

where ξ_s is the damping ratio for shear wave velocity V_s (m/s) in case 4. As shall be shown in later sections, since the 1D prediction results are sensitive to the damping level in the soil profile, adoption of such an empirical relation for Q_s is motivated by its effective application in several site response studies and the resulting intermediate site attenuation levels compared to other empirical relations and lab-based measurements.[55] In absence of better physical constraints, the P wave velocity V_p is calculated assuming a uniform Poisson's ratio $\nu = 0.3$ for the basin which gives $V_p = 1.87V_s$, and the P wave quality factor Q_p is determined as $2Q_s$ as commonly used in many past physics-based ground motion simulations.[56]

3.2 | Characteristics of the simulated ground motions

To examine the spatial variability of the performance of the simplified 1D approach in predicting the ground responses, horizontal and vertical ground motion time histories were recorded on a 500 m × 500 m surface grid on the basin side at various depths of the geologic profile, as shown in Figure 4B, resulting in a total of 3159 effective downhole array sites used in the assessment of 1D SRA, with a maximum rupture distance to the site of 20 km. Before performing detailed 1D analyses and site-to-site evaluations, it is important to have an overall sense of the quality of the simulated ground motions to ensure the motions are of engineering interest, and to gain insight into the characteristics of the true 3D site response which forms an important step in understanding the implications induced by the 1D approximation. For unknown (not historical) earthquake events as used in this study, Petrone et al.[57] proposed a four-step methodology and acceptance criteria to assess the reliability of simulated ground motions, involving comparisons of various ground motion

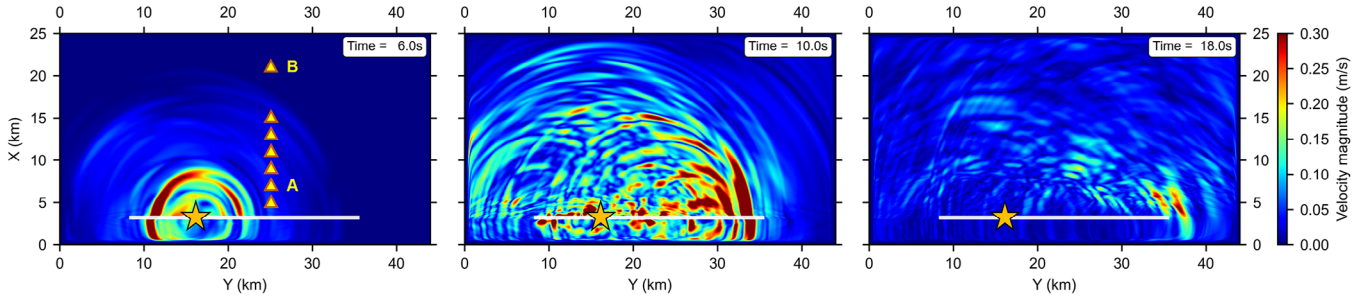

FIGURE 7 Snapshots of the simulated 3D seismic wavefield (surface velocity magnitude, plan view) in SW4 at three instants in time for the Mw 6.5 strike-slip event, case 1. The hypocentre is denoted by the star, and the white lines represent the fault projection on the ground surface.

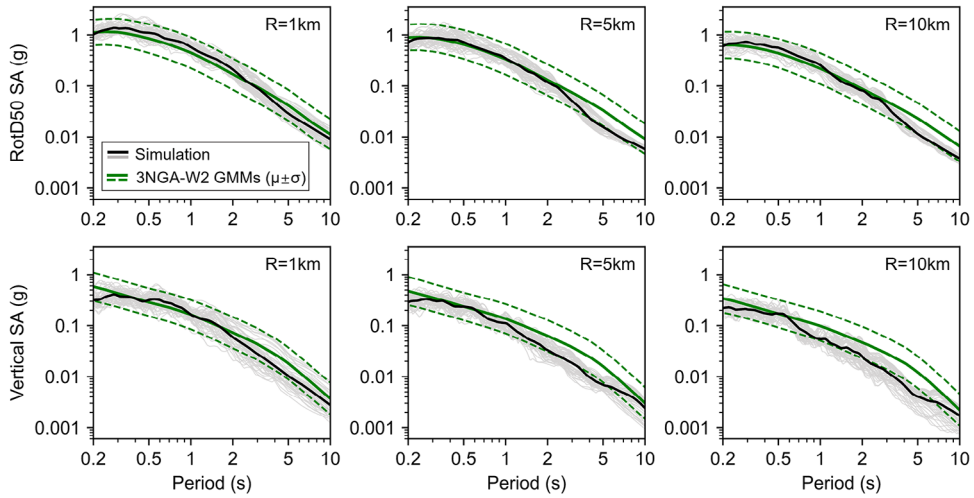

FIGURE 8 Spectral acceleration comparison of the simulated ground motions (case 1) and three NGA-West 2 ground motion models for the horizontal (RotD50, top row) and vertical (bottom row) components of surface motions for sites at rupture distances of 1 km (left column), 5 km (middle column), and 10 km (right column). The green lines represent the median ±1 standard deviation.

and engineering demand measures computed using simulated records, real records and empirical GMMs. Although a comprehensive evaluation of the simulated motions following the methodology proposed therein is out of the scope of this study and is not done here, for demonstration purposes, we summarize some of the major characteristics of the simulated ground motions from our 3D earthquake simulations for the baseline case 1 (Figure 6A).

Figure 7 displays snapshots of the simulated 3D seismic wavefield from SW4 for three instants in time that consecutively show the 3D wave propagation process starting from the initialization of the fault rupture, wave amplification in the basin and directivity effects towards the ends of the fault, and later-arriving surface waves propagating away from the basin edge. To quantitatively evaluate the amplitude of the simulated ground motions, we compare the 5% damped horizontal (orientation-independent RotD50[58]) and vertical spectral acceleration (SA) of the simulated records in Figure 8 with three pairs of NGA-West 2 GMMs that are developed for both ground motion components.[22,59–63] While the simulated motions at a particular site are expected to deviate from the empirical GMM estimates, the GMMs provide a useful check for the average ground motion intensity that are indicative of the seismic demand imposed on engineering structures. As shown in Figure 8, the median SA and ±1 standard deviation of the GMM estimates at three different rupture distances envelops most of the simulated records over a broad frequency band. The horizontal and vertical motions demonstrate somewhat lower intensities than the GMMs predictions in the long-period range, with the vertical component falling off faster compared to its horizontal counterpart. The observed deficiency in the long periods may be attributed to the simplistic shallow basin structure we have employed in the simulation, which underestimates long-period wave amplification occurring in some deep sedimentary basins that have constrained the development of empirical GMMs, or some limitations in the modelling of long-period wave energy by the kinematic rupture model used in this study.[40] Since vertical motions are more sensitive to the near surface heterogeneity compared to the horizontal component, small-scale velocity perturbations and

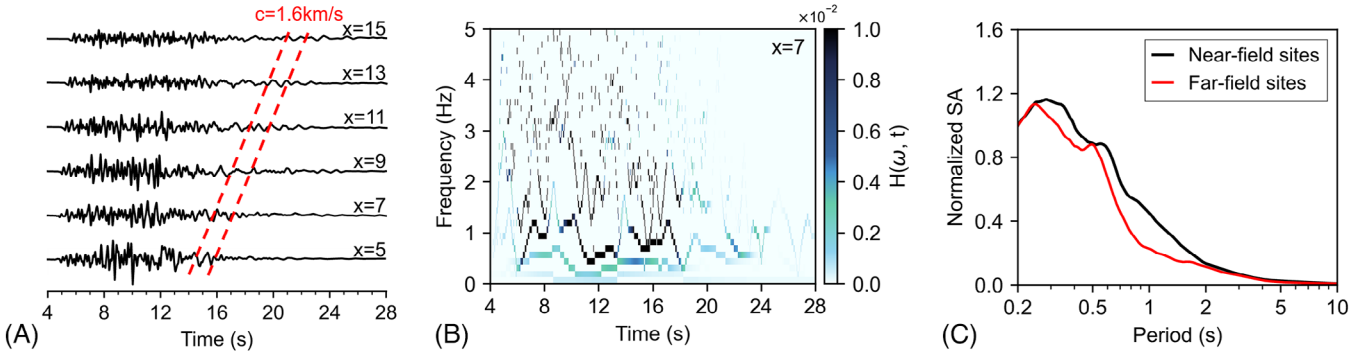

FIGURE 9 (A) Vertical accelerations at several sites normal to the basin edge ($y = 25$ km, yellow triangles in Figure 7 for 5 km $\leq x \leq$ 15 km) with an apparent surface wave velocity of 1.6 km/s; (B) temporal evolution of the frequency contents of the vertical acceleration at station $x = 7$ km in (A); (C) normalized median SA (with respect to SA at 0.2 s) comparison of motions at near-field sites (4 $\leq x \leq$ 8 km, 205 sites) and far-field sites (18 $\leq x \leq$ 23 km, 246 sites).

multiple layers with velocity contrast may improve the alignment of the simulated vertical motions and empirical GMM predictions (A. Pitarka, personal communication, June 27, 2023). A thorough evaluation of the effects of these potential influencing factors on the simulated ground motions statistics is, however, outside the scope of this study. Overall, the simulated ground motions are in reasonable agreement with the empirical GMM predictions in terms of spectral shape and distance attenuation, providing confidence in utilizing these motions for the evaluation of 1D SRA.

Past studies have shown that in sedimentary basins, surface waves are generated due to the wave mode conversion at the basin edge, and their constructive interference with the upgoing body waves can result in significant concentration of structural damage in the proximity region.[64] For demonstration purposes, Figure 9A shows the vertical accelerations along selected sites normal to the basin edge (yellow triangles shown in Figure 7 for 5 km $\leq x \leq$ 15 km). It is seen that the dominant surface wave packets are propagating with an apparent wave velocity of about 1.6 km/s (marked by the red dashed lines), much slower than the early-arriving P and S waves. Temporal evolution of the frequency contents of the vertical acceleration at station $x = 7$ km (Figure 9B) based on the Hilbert-Huang transform illustrates that the dominant frequency of the later-arriving surface waves is around 1–2 s. The influence of surface waves in the simulated ground motions is also observed through the comparison of the normalized spectral acceleration shape for the near-field sites (4 km $\leq x \leq$ 5 km, 205 sites) and far-field sites (18 km $\leq x \leq$ 23 km, 246 sites) shown in Figure 9C, where the long-period component for the near-field sites is significantly higher than that in the far-field. Although not shown here, surface waves generated in case 3 are more significant due to the large velocity contrast between the basin sediments and adjacent rock that results in more efficient wave mode conversions.

4 | 1D SRA WITH OUTCROP AND IN-COLUMN INPUT MOTIONS

To evaluate the applicability of the standard 1D modelling approach to site response predictions in shallow sedimentary basins, we performed linear-viscoelastic 1D wave propagation analyses based on the 1D assumption, that is, we assume the horizontal and vertical motions in the true 3D site response in SW4 are caused only by vertically propagating shear and compressional waves, respectively. For this purpose, we have conducted two types of 1D SRA using the two input-boundary pairs that are commonly employed in practice: (1) outcrop input motions paired with an absorbing boundary for the underlying half-space, and (2) the total in-column input motions recorded at the rock-basin interface paired with a fixed boundary at the base, also known as the within assumption. Without influence of the local surficial soils, the outcrop motions are considered to only contain the information of incident seismic waves, and half of the outcropping horizontal and vertical motions are used as the upgoing incident waves for the soil column in consideration of the free surface effect for assumed vertically propagating waves. In practice, the outcrop motions are typically recorded at or estimated for a nearby rock outcropping site while the in-column motions are usually recordings in a vertical downhole array. All the 1D analyses are performed using the Site2D program,[38] a verified and efficient Python code for linear-viscoelastic 1D and 2D wave propagation simulation in multilayered media.

In this study, a full SW4 simulation and a complementary SW4 run were performed to obtain the two types of input motions for 1D SRA, as shown in Figure 10. Figure 10A shows the full simulation case where the in-column input motions

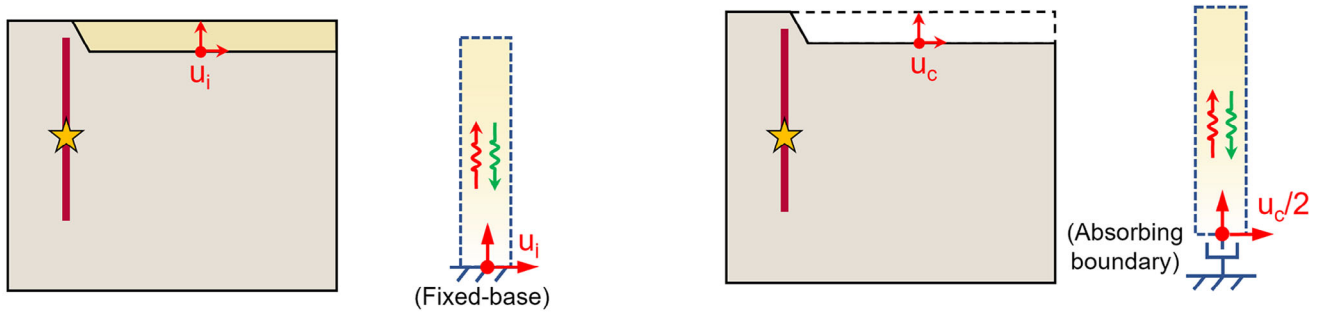

FIGURE 10 Input motions for 1D SRA: (A) In-column motion recorded at the basin-rock interface; (B) outcrop motion recorded on the ground surface from a complementary SW4 run of (A) that has the basin removed to simulate the rock outcropping condition.

at the basin-rock interface, as well as the reference 3D motions are computed in one pass. It is noted that for 1D SRA with in-column input motions, ground motions predicted in the 1D column is only dependent on the input motion at the base (i.e., not dependent on the geologic profile below), and recordings at any arbitrary depth below the site of interest can be used as the 1D input as long as the soil column is also cut at that depth. For the purpose of this study, we have chosen the motions at the basin-rock interface to consider the site effect induced by the full-depth soft sediments.[46,65] In Figure 10B, a complementary run with the same rupturing fault and crustal model as the full simulation case, except the shallow sedimentary basin was removed to simulate the rock outcropping conditions, was performed and the ground surface motions recorded at the same locations as for the in-column input motions were utilized as the corresponding outcrop motions. Since the geologic model and source-to-site setting were preserved in the complementary run, uncertainties induced by amplitude scaling of the outcrop input motions commonly needed when using actual records,[3] and implicit reliance on the 1D assumption when using a deconvolution analysis, are avoided in our investigations.[11] 1D SRA using the two types of input motions were performed for all the recorded basin sites in three directions, resulting in a total of 18954 1D analyses in the evaluation process for each basin profile case. For all the 1D site response analyses, we have employed frequency-independent damping that is consistent with the attenuation mechanism used in the 3D SW4 simulations. It is noted that since the soil profile is the same across the whole sedimentary basin, this uniformity allows for isolating the effects of wavefield characteristics due to 3D wave propagation on the spatial variability of the accuracy of the 1D modelling approach.

5 | ASSESSMENT OF 1D SRA COMPARED TO SIMULATED 3D SEISMIC WAVEFIELDS

The applicability of the 1D modelling approach is assessed through detailed frequency-domain comparisons of the transfer function (TF), the 5%-damped SA, as well as time-domain comparisons of various ground motion intensity measures (IMs) including the peak ground acceleration (PGA), the peak ground velocity (PGV) and the ground motion significant duration (D_s). In 1D SRA, the TF is typically calculated as the ratio of the Fourier amplitude spectrum of the surface motion to that of the input motion and determines how seismic waves at each frequency are amplified (or de-amplified) when propagating through the soil layers. We refer to the calculated TF as the 3D simulated transfer function if the surface motion at the site is obtained directly from the 3D earthquake simulation, or as the theoretical transfer function if the surface motion corresponds to the 1D SRA prediction. The PGA, PGV and D_s are indicators of the high-frequency components, intermediate-to-long-period components, and significant shaking duration of the earthquake record, respectively, and collectively provide an alternative approach for assessing the accuracy of the 1D approach across a broad range of frequencies in the time domain. In this article, the D_s is determined as the time difference between two chosen percentages on the normalized temporal accumulation curve of the Arias intensity (AI).[66]

Based on the comparison results, we evaluate the difference in the amplification mechanism of the horizontal and vertical site response in the canonical shallow basins. The implications of performing 1D approximations for 3D seismic wavefields including the prediction bias and spatial variability are identified, and the sensitivity to the sedimentary basin velocity and damping profiles are analysed. It is noted that since the results for different basin profiles show overall

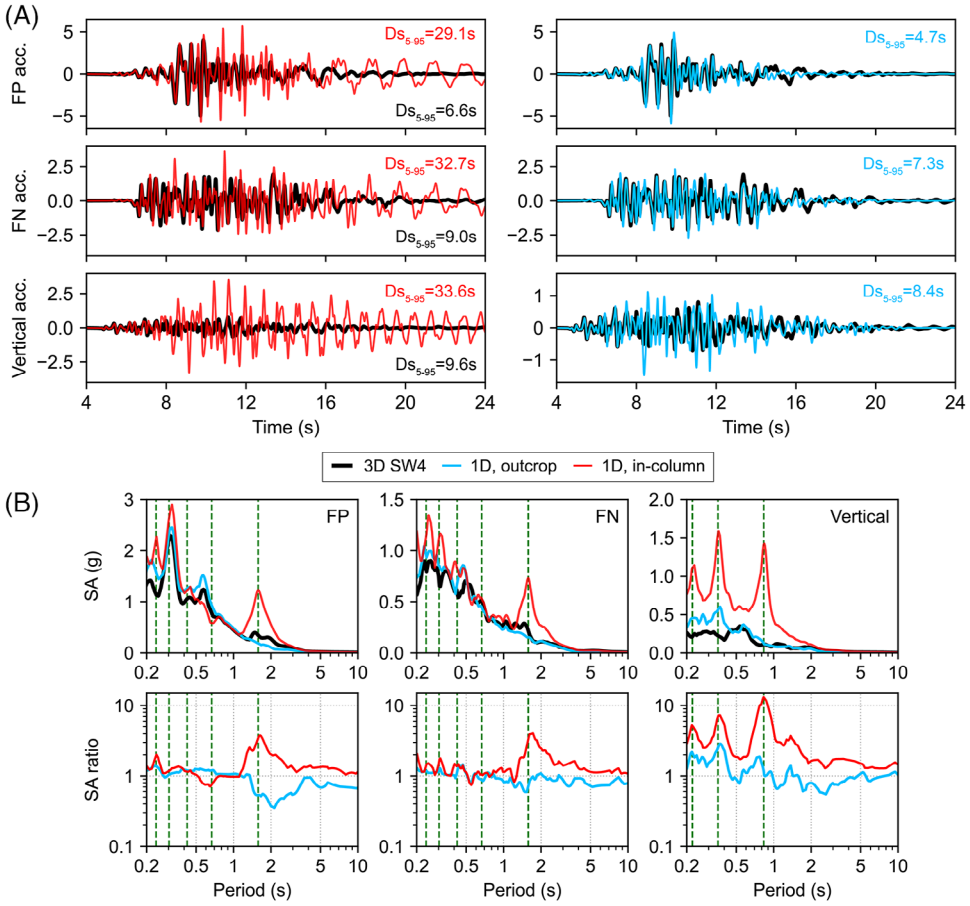

FIGURE 11 Comparison of surface acceleration and response spectra computed by the 3D SW4 simulation and 1D SRA with outcrop and in-column input motions in the fault-normal (FN), fault-parallel (FP) and vertical directions for a representative site A ($x = 7$ km, $y = 25$ km in Figure 7) in case 1: (A) Surface acceleration (unit in m/s^2), and $D_{s5\text{-}95}$ (the three cases are denoted by the respective colours); (B) SA and the SA ratios of the 1D predictions to the reference 3D SW4 solution where the green dashed lines indicate the site periods in the respective directions.

similar trends, results from the baseline case 1 are used in the following sections for demonstration purposes unless specified otherwise.

5.1 | Amplification mechanism of the horizontal and vertical site response

As noted in the Introduction, field observations have suggested different levels of accuracy of 1D SRA for the horizontal and vertical motion estimations, indicating the deviation of the actual 3D site response from that based on the 1D assumption, especially in the vertical direction. In this section, we evaluate the amplification mechanism of the horizontal and vertical motions in the simulated 3D seismic wavefields in detail, with a focus on the discrepancy between the amplification mechanism in the true 3D site response and that assumed in 1D SRA and the corresponding implications for the 1D prediction bias.

To have an overall sense of the accuracy of the simplified 1D modelling approach for the simulated 3D seismic wavefields, we first show in Figure 11 the comparison of surface motions obtained directly from the 3D SW4 simulation and the corresponding 1D SRA predictions for a representative site A (see Figure 7). The surface motion comparison is shown in terms of the acceleration time history, SA, the SA ratios of the 1D predictions to the reference 3D solution, and the 5%−95% ground motion significant duration ($Ds_{5\text{-}95}$) for the fault-normal (FN), fault-parallel (FP) and vertical directions. For the two horizontal directions, it is seen that the 1D SRA predictions agree reasonably well with the reference 3D solutions in terms of both time history waveforms and SA, suggesting that the 1D assumption of vertically propagating S waves is largely valid at this site to capture the major horizontal wave arrivals. In the vertical direction, however, except the early P wave arrivals (i.e., before about 6.6 s), the vertical motions predicted by the 1D P wave propagation model with both

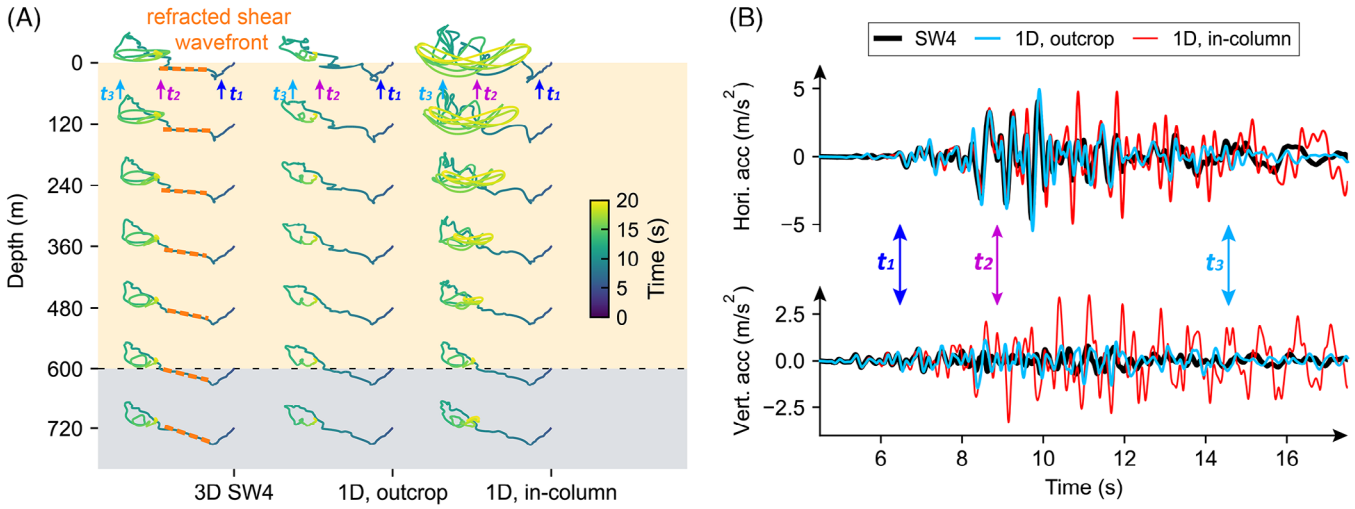

FIGURE 12 Comparison of (A) particle movements and (B) surface accelerations from the 3D wavefield in SW4 and two 1D SRA predictions at station A in case 1. Note the horizontal motions at the station are rotated to the radial and transverse directions with respect to the epicentre location, and the horizontal motion shown in the figure are the radial component. t_1, t_2 and t_3 denote the end of the P wave window, the end of the first major S wave arrival and the end of S wave arrivals, respectively, and the orange dashed lines show the gradual refraction of the first major S wavefronts when propagating towards the surface.

types of input motions are not consistent with, and are significantly larger than, the reference 3D SW4 motion in the S wave window, implying that the assumed 1D P wave propagation model does not capture the physics of the actual vertical site response. It is noted that, because of wave trapping in the 1D soil column, 1D SRA using the in-column input motion have predicted horizontal and vertical motions with much longer duration due to the multiple reverberations in the later phases that do not exist in the reference 3D solutions, resulting in much larger amplification near the site periods. For instance, in the FP direction, the $Ds_{5\text{-}95}$ ratio of the surface motion by 1D SRA to that of the 3D solution is about 4.4 (i.e., 29.1 s/6.6 s) and the SA ratio at the site fundamental period ($T = 1.58$s) reaches 3.6 (i.e., 1.22g/0.34 g). When using the outcrop input motion, it is observed that 1D SRA underpredicts $Ds_{5\text{-}95}$ and SA beyond about 1.3 s due to its inability to capture the later-arriving basin-edge generated surface waves and the wave mode conversions within the soil layers. Although the 3D-1D comparisons shown here are based on results for site A, it should be noted that these observations are in general common for sites across the entire computational domain.

To investigate the cause of the vertical motion over-prediction bias observed at site A, we plot in Figure 12 the particle movements of the reference 3D solution and two 1D SRA predictions at different depths and the surface motion time histories. Note the two horizontal surface motions at this site are rotated to the radial and transverse directions with respect to the epicentre location to better isolate the P-SV waves that contribute to both the horizontal and vertical motions, and the results are plotted in the radial-vertical plane. Since the near-fault permanent displacements are fully captured in the 3D earthquake simulation, this offers an opportunity to delineate and examine the particle motion in the P and S wave windows separately. As seen in Figure 12A, the particle movement in the true 3D site response solution can be coarsely attributed to three wave arrival phases, that is, the early P wave arrivals before t_1 characterized by particle movements parallel to the wave propagation direction, the major S wave arrivals between t_1 and t_3 represented by particle movements normal to the propagation direction, and the later surface wave arrivals after t_3 showing elliptical trajectories. Of most interest here is the S wave window where both the peak horizontal and vertical accelerations reside, demonstrating the significant contribution of the S waves to both components of the wavefield, and where the over-prediction of the vertical motion occurs. For illustration, we focus on the difference in the 3D and 1D site response for the first major S wave arrival (t_1–t_2), the wavefronts of which are traced with the orange dashed lines across the depth. When the inclined incident S wave propagates upwards, due to the velocity gradient in the basin soil profile, the induced 3D site response consists of a first-arriving converted P wave[67] and the later gradually refracted direct S wave, with the vertical acceleration caused by the direct S wave dominating the vertical motion because of the large S wave amplitude. As a result, the vertical site response is coupled with the horizontal site amplification through the refraction process. However, in the 1D estimation of the vertical motion, since the input motion for the 1D P wave propagation model is obtained at depth (or on the surface for an outcrop motion) where the incident S wave is more inclined and has larger vertical component compared to that

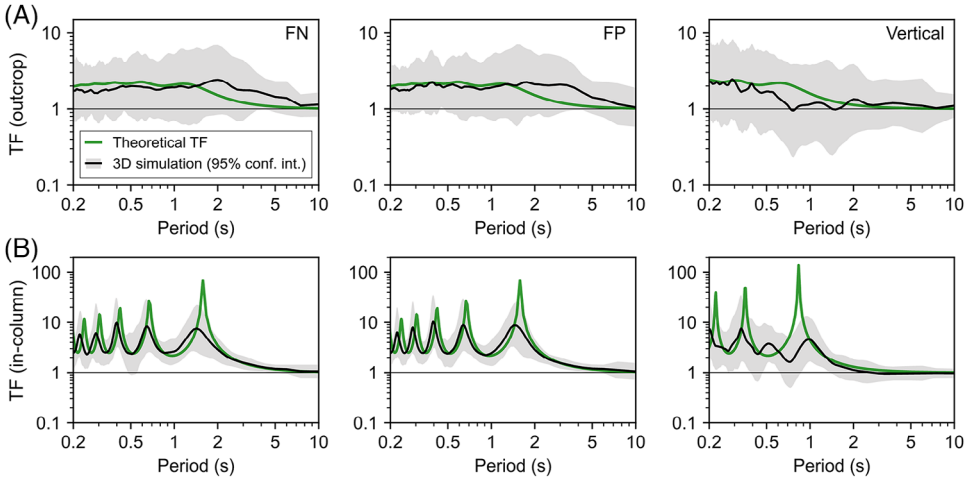

FIGURE 13 Comparison of the theoretical and 3D simulated TFs of case 1 calculated in the FN, FP and vertical directions when assuming: (A) outcrop boundary condition; (B) in-column boundary condition. The black line and the grey area represent the median plus/minus two standard deviations (i.e., 95% confidence interval).

when it reaches the surface, this has led to a strong P wave arrival and later reverberations at the surface much larger than that in the true 3D site response, leading to the consistent vertical motion over-prediction at this site with both types of input motions.

The 3D-1D comparison results at site A demonstrate that the horizontal motions at the site are predicted by the 1D approach with reasonable accuracy, while the vertical motion is over-predicted because of the significant contribution of inclined S waves to the vertical site response. To examine the generality of these observations at the remaining sites, we show in Figure 13 the comparison of the theoretical TFs obtained based on the 1D assumption and the 3D simulated TFs calculated using the reference motions directly from SW4 for all sites in the domain. Since the theoretical TF for a 1D model is only a function of the velocity and damping profiles (i.e., not dependent on the input excitation), it is often used as a proxy to evaluate the deviation of the actual site response from the assumed 1D model. As illustrated by Figure 13, the overall good agreement between the theoretical TFs and the median 3D simulated TFs in the two horizontal directions, and the large discrepancies in the vertical direction, confirm from a statistical perspective that the horizontal site amplification is dominated by the 1D S wave propagation behaviour as assumed in 1D SRA, while the vertical site amplification is complicated by the large contribution of inclined S waves. The existence of inclined shear waves is also evidenced by the shift of the frequencies at which the horizontal 3D simulated TFs peak towards higher frequencies compared to the theoretical TFs calculated assuming the in-column boundary condition. This is explained by the fact that inclined waves effectively travel shorter paths than the full soil column depth of the assumed 1D model (refer to Figure 3B), leading to wave destructive interference at the base occurring at shorter periods.[68] It is also observed that the theoretical TFs calculated assuming the outcrop boundary condition tend to under-predict the 3D motions beyond about 1.3 s due to the lack of modelling of the surface waves. For the vertical direction, the overall over-prediction of the TFs across nearly the entire period range suggests persistent vertical motion over-prediction when using both types of 1D input motions.

When using the in-column input motion, it is shown in Figure 13 that the theoretical TFs demonstrate sharper peaks near the site periods compared to that in the 3D simulation. Similar observations have also been made in past site response studies based on instrumented downhole arrays.[47,65] It is well recognized that, for vertically propagating waves passing through horizontally layered soil profiles, destructive wave interferences between the upgoing incident wave and the downgoing reflected wave from the surface can occur at certain frequencies at a given depth, known as the downgoing wave effect,[69] leading to local minimums in the spectral acceleration at these frequencies. For site amplification more prone to the 1D wave propagation behaviour, this downgoing wave effect is expected to be more pronounced. For a point at depth h in a homogenous half-space, the frequencies f_d at which the destructive wave interference occurs can be calculated by[69] $f_d = \frac{(2n-1)v}{4h}$, where v is wave velocity and $n = 1,2,3,\ldots$. For the inhomogeneous soil profile used in the sedimentary basins, we can obtain f_d numerically by performing 1D SRA with the outcrop motion and calculating the transfer function between the motions at depth and the outcrop input motion, and f_d then corresponds to the frequencies at which the troughs of the transfer function occur. To examine the possible cause of the sharp peaks in the theoretical in-column TFs

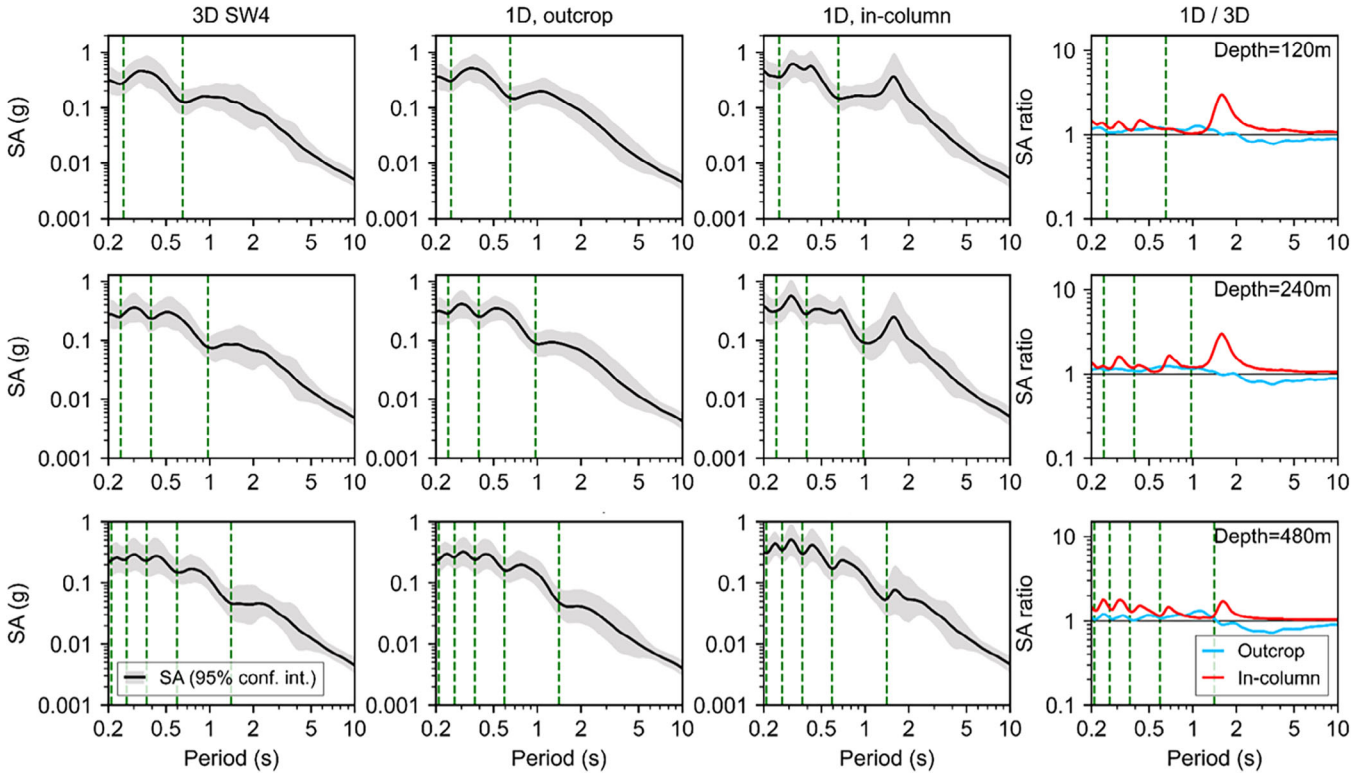

FIGURE 14 SA of the horizontal motions (RotD50) from the 3D SW4 simulation and the corresponding 1D SRA predictions, along with the SA ratio of 1D to 3D at depths of 120 m (top row), 240 m (middle row) and 480 m (bottom row). Note the motions are for sites 5 km away from the fault in case 1; the black line and the grey area represent the median value plus/minus two standard deviations of SA (i.e., 95% confidence interval); the SA ratios are the median value of all considered site; and green dashed lines indicate periods that correspond to troughs in the theoretical 1D transfer functions for motions at different depths.

and evaluate the closeness between the 3D site response in SW4 and the assumed 1D site amplification along the whole soil profile, we show the SA of the horizontal and vertical motions at sites 5 km away from the fault line in Figures 14 and 15, respectively, along with the spectral ratio of the 1D prediction to the 3D reference solution. The green dashed lines in the plots correspond to f_d for motions at the respective depths. A preliminary analysis shows that ground motions at different distances from the fault also give similar observations. As can be seen in Figure 14, the horizontal motions from 3D SW4 show local SA minimums at frequencies f_d, indicating similar destructive wave interferences along the soil profile as in the 1D S wave propagation model, although the local troughs near f_d observed in the horizontal SA ratio suggest these destructive interferences are less strong compared to that obtained in the 1D analysis, in agreement with the observed smaller peaks in the TFs from the 3D simulation. Except the wave trapping-induced over-amplification near the site periods when using the in-column input motion, the amplitude of the horizontal SA at different depths are captured reasonably well by the 1D analyses using the two types of input motions. In contrast, vertical motions from 3D SW4 are not only much smaller than the corresponding 1D predictions at different depths, but also show flattened troughs in the SA and more significant valleys in the SA ratio near frequencies f_d predicted with the 1D P wave propagation model, implying much less significant destructive wave interferences than the horizontal components. These observations suggest that the artificially stronger destructive wave interference enforced by the 1D model has led to the stronger peaks in the theoretical 1D TFs, and for the shallow sedimentary basins considered in this study, in general, the horizontal motions are dominated by shear waves, while the vertical motions are a combination of shear and compressional waves and 1D SRA will lead to vertical motion over-prediction bias over the entire soil column.

5.2 | Spatial variability of the accuracy of the 1D modelling approach

As demonstrated in the previous section, the horizontal and vertical site response show different amplification mechanisms due to the distinct wave composition that contributes to the two components in the 3D wavefield. For the Mw

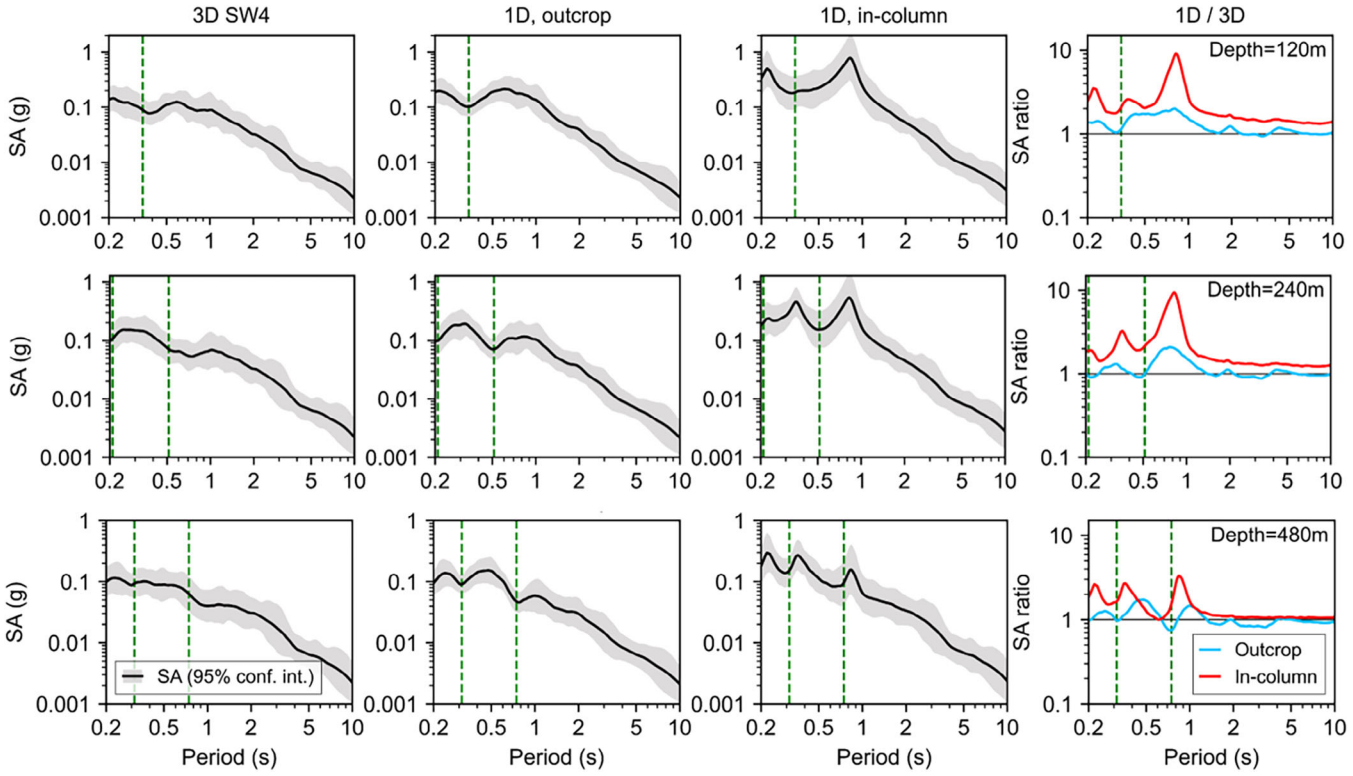

FIGURE 15 Same as Figure 14 except the results are for the vertical motions.

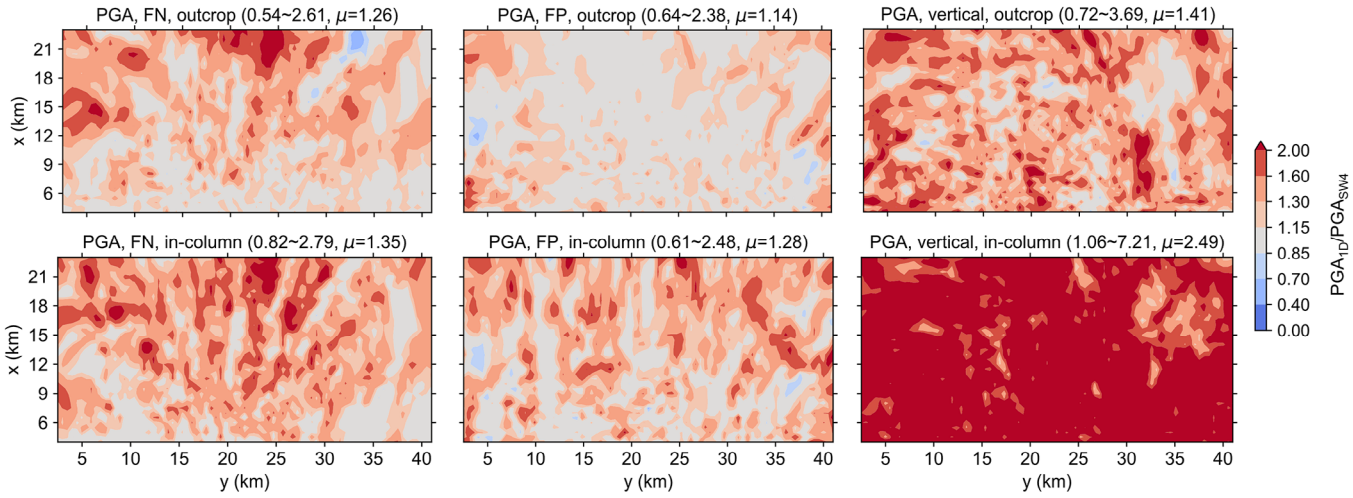

FIGURE 16 PGA ratios of the 1D SRA predictions to the reference 3D SW4 solution (case 1) for surface motions in the FN, FP and vertical directions when using outcrop input motions (top row) and in-column input motions (bottom row). The values in the parenthesis for each subplot are the minimum, maximum and median of the ratios, respectively.

6.5 strike-slip earthquake scenario considered in this study, the fault rupture process is modelled explicitly with realistic spatially distributed kinematic rupture properties. Since the composition of the wavefield varies spatially because of the complex interferences of seismic waves emitted from different portions of the rupturing fault, both in the reference 3D surface motions and the input motions for 1D SRA, the accuracy of the 1D approximation to the 3D wavefield is expected to be site dependent. Figures 16–18 show the ratios of the 1D SRA predictions to the reference 3D solutions for the PGA, PGV and the 5%~95% significant duration $Ds_{5\text{-}95}$ in the FN, FP and vertical directions, along with the statistics of the ratio (minimum, maximum and median values) for all sites in the domain.

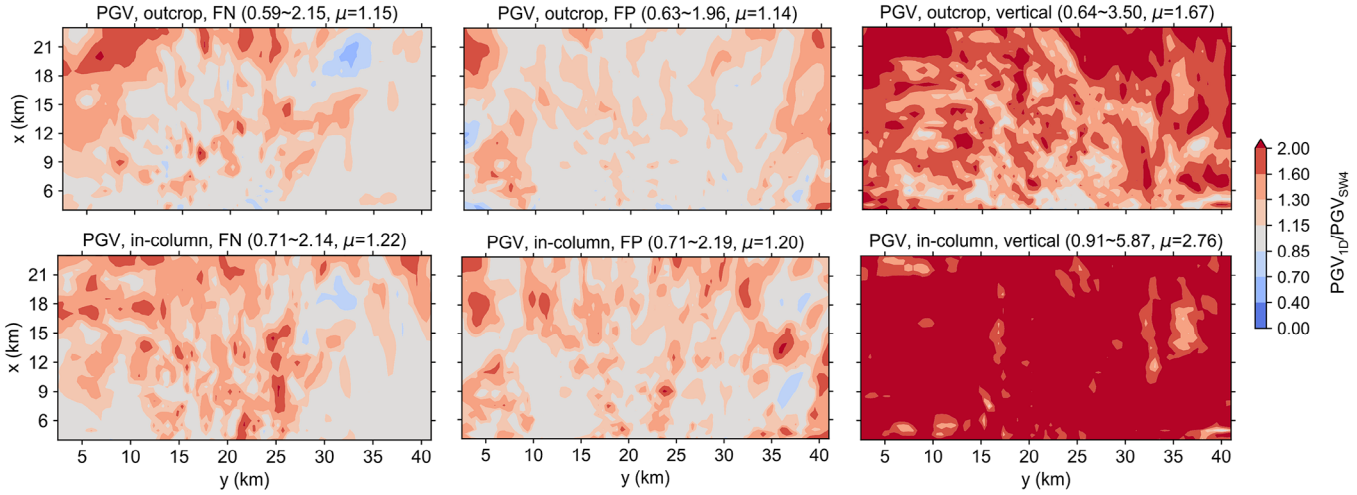

FIGURE 17 PGV ratios of the 1D SRA predictions to the reference 3D SW4 solution (case 1) for surface motions in the FN, FP and vertical directions when using outcrop input motions (top row) and in-column input motions (bottom row). The values in the parenthesis for each subplot are the minimum, maximum and median of the ratios, respectively.

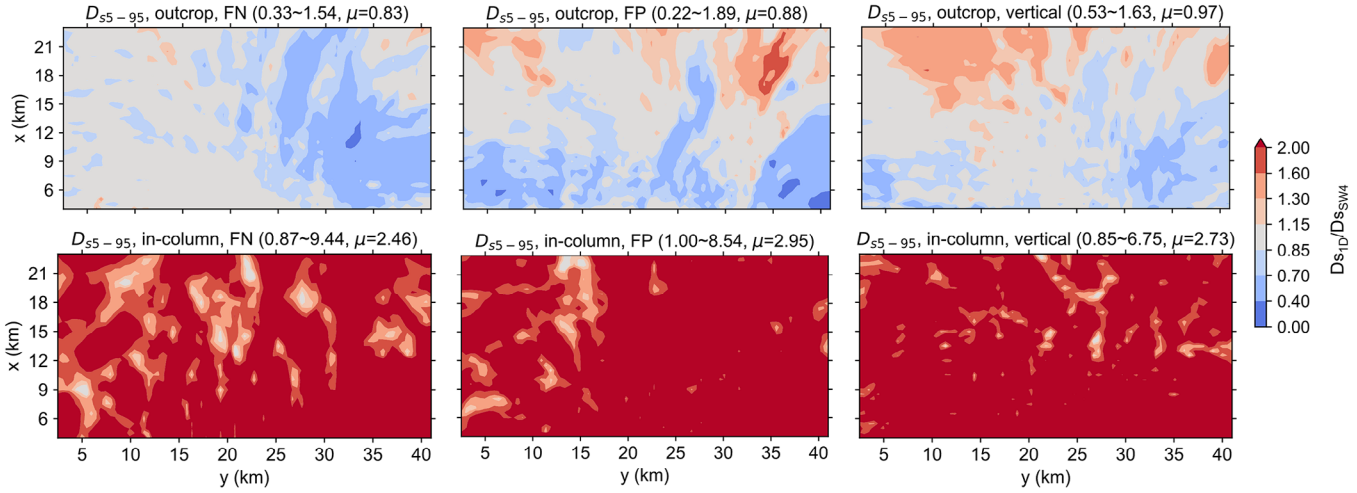

FIGURE 18 $D_{s5\text{-}95}$ ratios of the 1D SRA predictions to the reference 3D SW4 solution (case 1) for surface motions in the FN, FP and vertical directions when using outcrop input motions (top row) and in-column input motions (bottom row). The values in the parenthesis for each subplot are the minimum, maximum and median of the ratios, respectively.

Compared to the reference 3D solution, the simplified 1D approach tends to over-predict PGA, PGV in both the horizontal and vertical directions (i.e., ratios larger than one) and this phenomenon is much more pronounced in the vertical component. For 1D SRA with outcrop input motions, underprediction of $Ds_{5\text{-}95}$ occurs at sites near the basin edge due to the insufficient representation of surface waves that is not modelled with the simplified 1D approach. Although not shown here, this underprediction is more significant for basin profile case 3, where surface waves are more prominent in the 3D wavefield due to the larger rock-basin impedance contrast at the basin edge. It is interesting to note the apparent dependency of the 1D accuracy on the site distance to the fault, that is, the increased level of over-prediction with increasing distance to the fault, as seen for the prediction of PGA and PGV in the two horizontal directions with both outcrop and in-column input motions, and the prediction of PGV in the vertical direction using the outcrop input motion.

This spatial variability is also illustrated in Figure 19 where we plot the SA ratios of the 1D SRA predictions to the reference 3D SW4 solution for surface motions at the near-field (4 km $\leq x \leq$ 5 km) and far-field (18 km $\leq x \leq$ 23 km) sites. Note the motions in the FP direction give similar results as the FN direction and are not shown for brevity. Compared to the near-field sites, the overall over-prediction bias for the FN and vertical motions at the far-field sites is more significant. Furthermore, the horizontal and vertical directions show different characteristics, that is, the period range over which

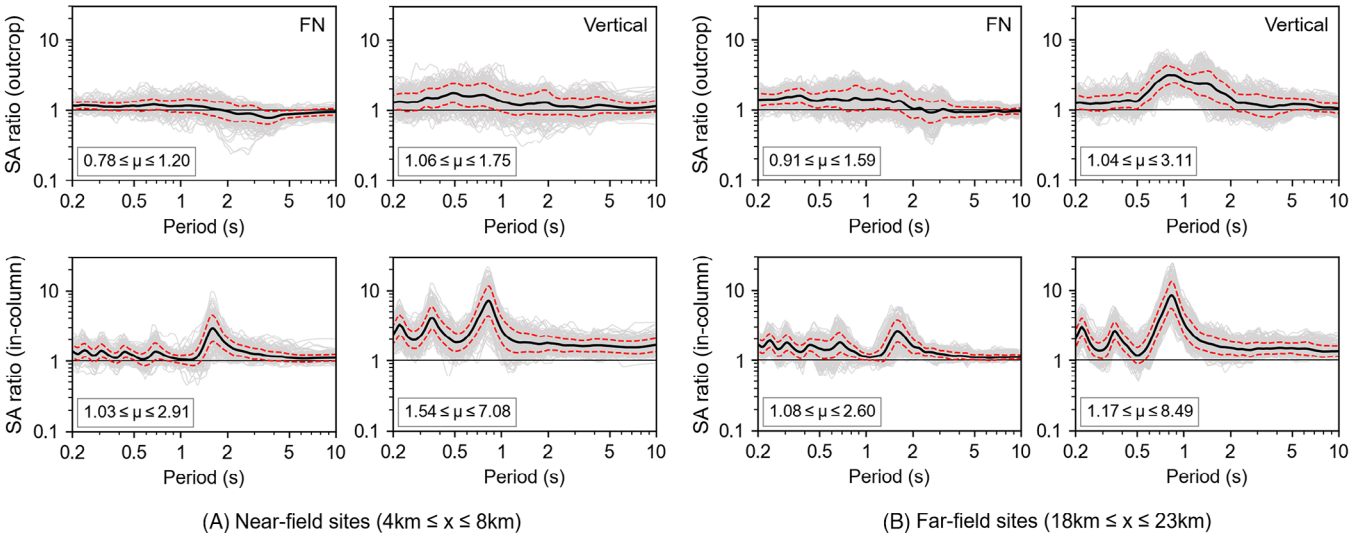

FIGURE 19 SA ratios of the 1D SRA predictions to the reference 3D SW4 solution (case 1) for surface motions in the FN and vertical directions at (A) near-field sites; (B) far-field sites. In each panel, the first and second rows are for SA ratios using the outcrop and in-column input motions, respectively; the solid black lines and dashed red lines represent the median SA ratio (μ) ±1 standard deviation; the values in the text box show the range of μ.

the most prominent over-prediction occurs is shifted towards shorter periods for the horizontal component and shifted towards longer periods for the vertical component.

The observed spatial variability of the 1D performance in predicting the 3D site response is attributed to the variation in the characteristics of the input motions across the domain, including both the wavefield composition and the temporal evolution of the frequency content. Since P and S waves emitted from the source cannot be physically separated, for verification purposes, we have conducted a numerical experiment where we set the P wave damping for the entire layered crust (except the sedimentary basin) to be 10% and performed the full SW4 simulation and the corresponding complementary run (Figure 10B) to obtain the outcrop and in-column input motions. Since the finite difference scheme in SW4 requires decreased time step for increased viscoelasticity to ensure numerical stability,[48] the high P wave damping value for the layered crust was chosen to largely damp out the incident P waves in both the outcrop and in-column input motions such that the contribution of the incident P and S waves can be separately assessed in the evaluation process without incurring an excessively large penalty for increased computational efforts. As an example, we show in Figure 20 the comparison of the outcrop and in-column input motions at the near-field site A and the far-field site B (see Figure 7) for case 1 with the original and modified crustal P wave damping (uniformly 10%). Three observations can be made in terms of the characteristics of the 1D input motions:

1. The horizontal and vertical input motions have contributions from both the P and S waves. Overall, S waves dominate the amplitude of both the horizontal and vertical incident motions, while the P waves have larger contribution to the vertical component.
2. The relative P wave contribution to both the total outcrop and in-column incident wavefields increases with distance to the fault as S waves are attenuated faster than P waves.
3. Compared to input motions at the near-field site A, input motions at the far-field site B have more time separation between the P and S wave windows due to the difference in the P and S wave speeds. Because of the strong S wave attenuation with distance, comparing Figure 20B and D, the dominant frequencies in the S waves are shifted towards lower frequencies that are closer to the vertical fundamental site period of the 1D column (denoted by the green dashed lines in Figure 11B).

Figure 21 shows the 3D-1D comparison of the surface motions at site B for SW4 simulation cases with the original and modified (uniformly 10%) crustal P wave damping. Based on Figures 11 and 21A, it is observed that as an effect of approximating the inclined P waves as vertically propagating S waves in the horizontal 1D SRA, the FN motion is more severely over-predicted by 1D SRA at site B compared to site A due to the increased contribution of P waves in the horizontal input

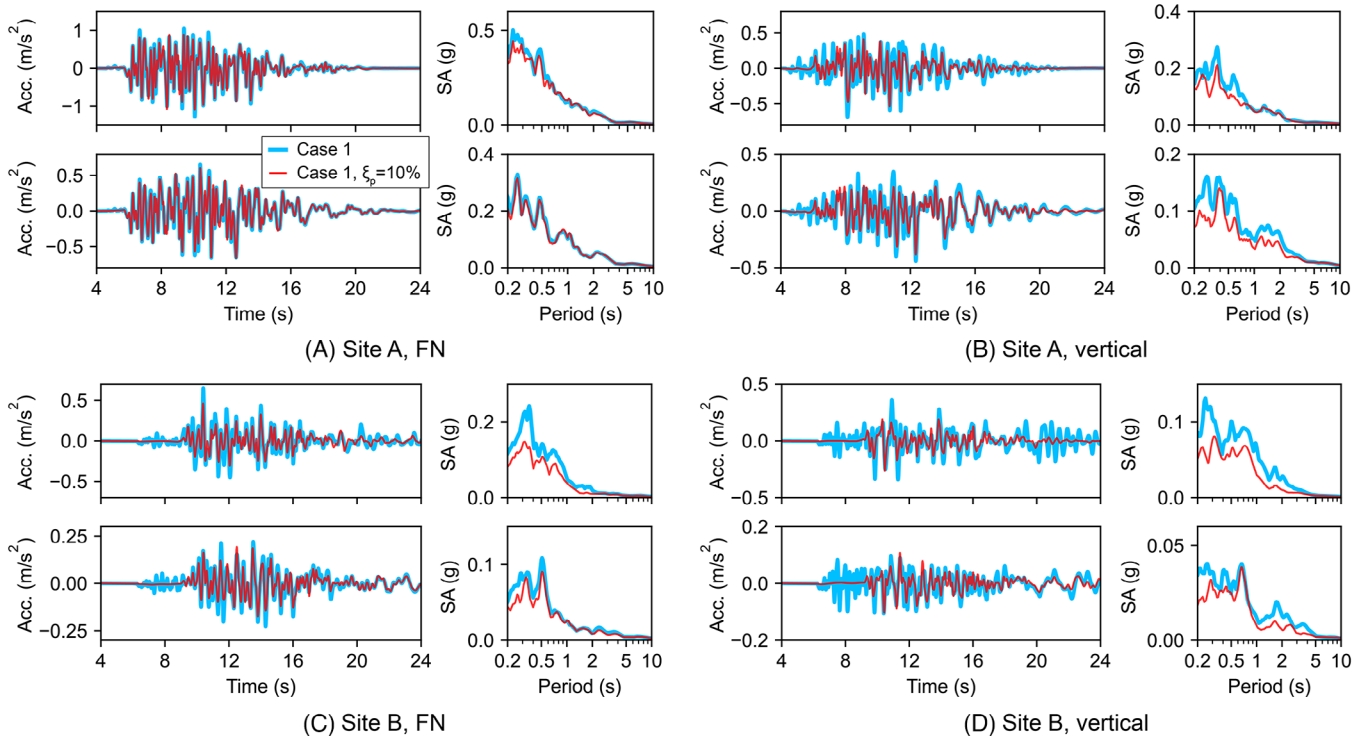

FIGURE 20 Comparison of input motions for sites A and B from SW4 simulations for case 1 with the original and modified (uniformly 10%) crustal P wave damping: (A) and (B) are for the FN and vertical directions of site A, respectively; (C) and (D) are for the FN and vertical directions of site B, respectively. In each panel, the first row shows the time history and response spectra for the outcrop motions, the second row shows the time history and response spectra for the in-column motions.

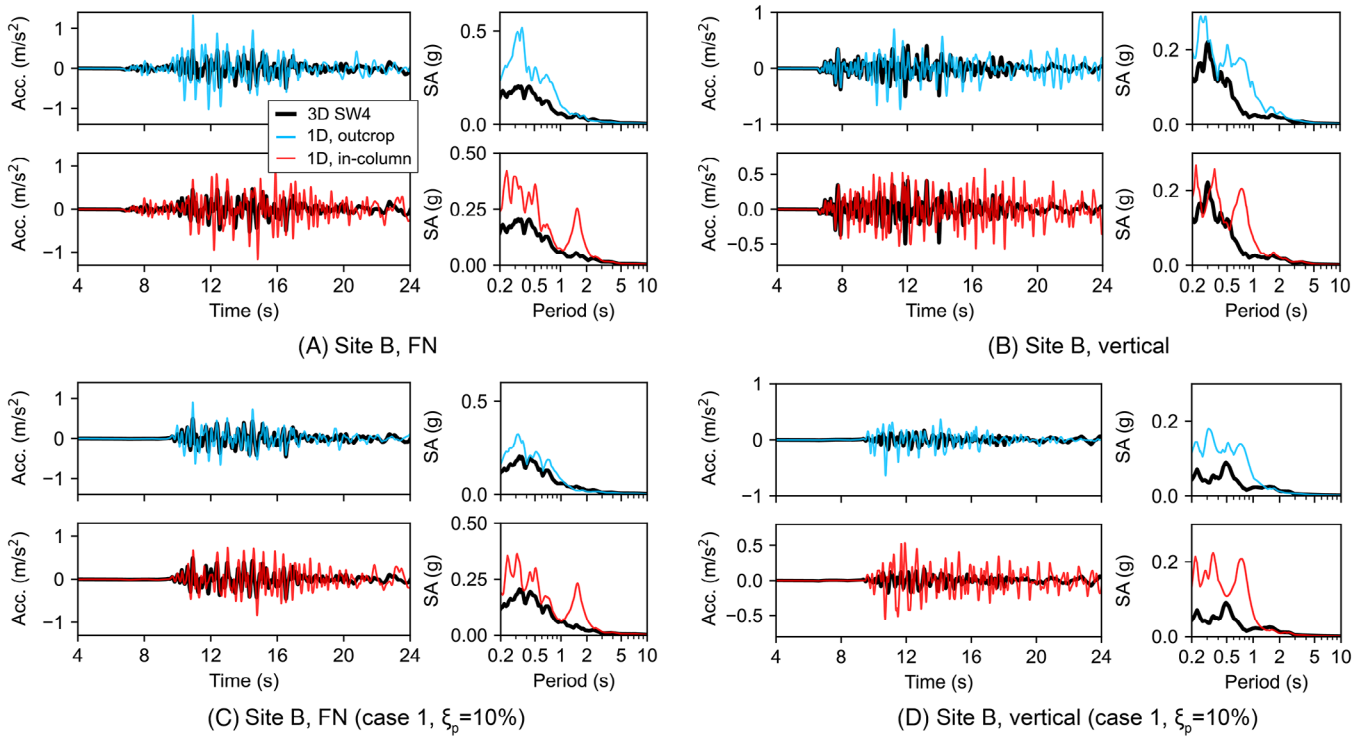

FIGURE 21 Comparison of surface motions in the FN and vertical directions at site B computed by SW4 and two corresponding 1D SRA predictions. The reference 3D motions are from SW4 simulations for case 1 with the original (A and B) and modified (C and D) crustal P wave damping (uniformly 10%).

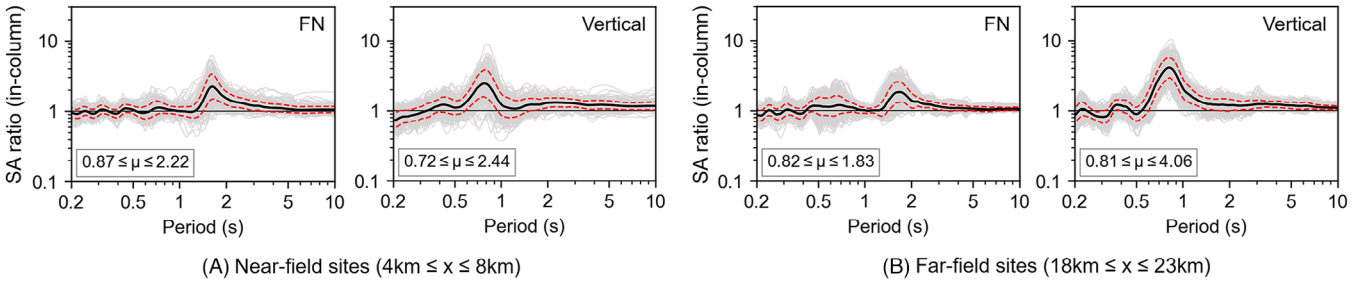

FIGURE 22 SA ratios of the 1D SRA predictions computed with the in-column motion and optimized damping to the reference 3D SW4 solution for surface motions in the FN and vertical directions at (A) near-field sites, and (B) far-field sites in case 1. In each panel, the solid black lines and dashed red lines represent the median SA ratio (μ) ±1 standard deviation; the values in the text box show the range of μ.

motions. On the other hand, the over-prediction of vertical motions shows distinct characteristics between sites A and B that warrants further explanation. Since the over-prediction of the vertical motions is driven by the large contribution of S waves in the 1D input motions, the shift in the frequency contents of the S waves towards lower frequencies in the input motions has led to more pronounced over-prediction of SA near the fundamental period of the 1D column for site B compared to site A. Conversely, due to the larger time separation between the P and S wave windows at the far-field site B, there is less possibility for constructive wave inference of P and S waves at higher frequencies, leading to less significant over-prediction of the vertical PGA at site B compared to the near-field site A. The implications of P wave contribution to the 1D SRA input motions become clearer when the incident P waves impinging on the soft soil layers is removed, as shown in Figure 21C and D. As expected, with reduced P wave contribution, S waves contribute more to the wavefield and this leads to improved prediction of the horizontal component and exacerbated prediction of the vertical component by the 1D approach. As can be seen, the actual performance of 1D SRA in approximating the 3D wavefields depends on both the wavefield composition and temporal evolution of the characteristics of the 1D input motions.

It is worth mentioning that due to the upper crustal velocity gradient, the incident angle of S waves remains relatively small when arriving at the base of the basin. For example, 3D ray tracing shows that for the seismic wave bursts emitted from the hypocentre, the incident angle of the S waves arriving at the rock-basin interface near the edge of the considered computational domain is about 33.9°, which is only marginally larger than the critical incident angle 27.8°. As mentioned in the Introduction, although the 1D approach has a tendency to under-predict the response of inclined seismic waves at large incident angles, under-prediction of the horizontal surface motions is not widely observed using the simulated ground motion datasets in this study.

5.3 | Sensitivity of wave trapping in the 1D column to the damping profile

In existing literature, including investigations on the accuracy of the 1D modelling technique, the damping profile of the site is often optimized to empirically match the field records due to the lack of measured attenuation parameters, for example, through a grid search of damping multipliers D_{mul} intended for scaling of the small-strain damping profile typically determined based on laboratory measurements. In this section, we follow a similar optimization procedure based on D_{mul} to examine the sensitivity of wave trapping to the damping level used in 1D SRA. Specifically, we perform 1D SRA for all the sites in the domain with D_{mul} ranging from 0.1 to 20 for the horizontal motions and 0.1 to 40 for the vertical motions, and choose respective D_{mul} values for the two components that result in lowest misfit between the SA of the 1D solution and 3D solution for periods within 0.2–0.5 s. It is noted that the value ranges for D_{mul} is determined based on a preliminary analysis to encompass the maximum damping levels needed in the optimization for most sites while keeping the maximum damping ratio below a reasonable limit (~60% in this case); the range for the SA periods is chosen to be in the short-period range such that the optimization is not overly weighted by the large discrepancies near the site periods, and the PGA before and after optimization remain approximately on the same level due to its strong correlation with the high-frequency components. In view that the wave trapping phenomenon is most prominent with the in-column (within) boundary condition which has been employed in most downhole arrays site response studies, for brevity, we show in the following the 1D SRA results with the in-column input motion only.

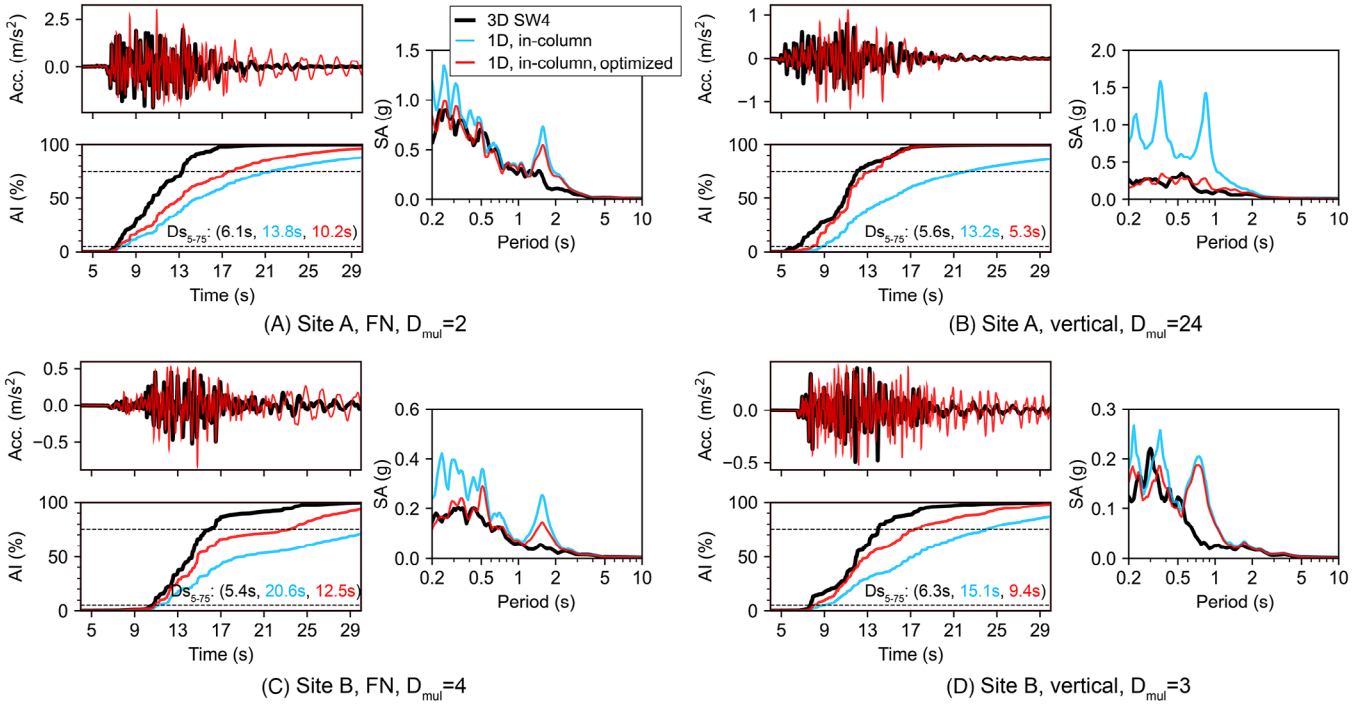

FIGURE 23 Comparison of surface motions from the reference 3D solution in SW4 for case 1, and two 1D SRA predictions with in-column input motions using the original and optimized damping profiles for the FN (A) and vertical (B) directions at site A, and for the FN (C) and vertical (D) directions at site B. In each panel, the optimized damping multiplier is shown in the subtitle; the three values in parenthesis are the 5%∼75% significant duration $Ds_{5\text{-}75}$ calculated for motions from SW4, and the two 1D SRA predictions using the original and optimized damping profiles, respectively.

In Figure 22, we show the SA ratios of the optimized 1D predictions to the reference 3D motions from SW4. Compared to the SA ratios with the original damping as shown in Figure 19, the match between the 1D and 3D solutions for both near-field and far-field sites are greatly improved across a broad period range, although large amplification near the fundamental site periods persists due to the exclusion of these long periods in the optimization process. To have a more detailed examination of the effect of increasing the small-strain damping on the accuracy of 1D SRA, as an example, Figure 23 shows the comparison of surface motions from the reference 3D solution in SW4 and two 1D SRA in-column predictions at sites A and B using the original and optimized damping profiles for the FN and vertical directions. It is noted that the optimized D_{mul} values for the four 1D analyses in Figure 23 are larger than 1, meaning that increased damping is needed for improved fit with the reference 3D motions for both the horizontal and vertical components due to the over-prediction in the 1D solutions. With the optimized damping, the 1D predictions for both the SA and the temporal accumulation of Arias intensity (AI) are improved, although the comparison of waveforms does not necessarily improve, especially in the vertical direction. For example, at site A, compared to results in Figure 11, the 1D predictions of SA and AI in the vertical direction have been greatly improved with a D_{mul} value as 24, while a detailed examination of the waveforms reveals that the improvement takes place mainly in the S wave window in terms of the matching of the overall amplitude instead of the individual wave arrivals, and the early P wave arrivals are underestimated by the 1D approach because of the large D_{mul} value employed. This indicates that although increasing the damping may improve the prediction of some ground motion intensity measures, it is an empirical rather than a physical approach. The increase of damping will only alleviate the phenomenon but cannot eliminate it as it is not the root cause. Since the wave interference is dependent on the characteristics of the input motions, optimization using D_{mul} will need to be conducted on a site-to-site basis and is not expected to give the same level of improvement, an example of which is observed at the far-field site B. As can be seen, due to the less significant constructive wave interference in the high frequencies of the vertical motion caused by the time separation between the P and S wave windows, optimization for SA is satisfied with a much smaller D_{mul} (= 3) compared to that at site A and this leads to overall minor improvement in the predicted surface motions in terms of both the response spectra and waveforms.

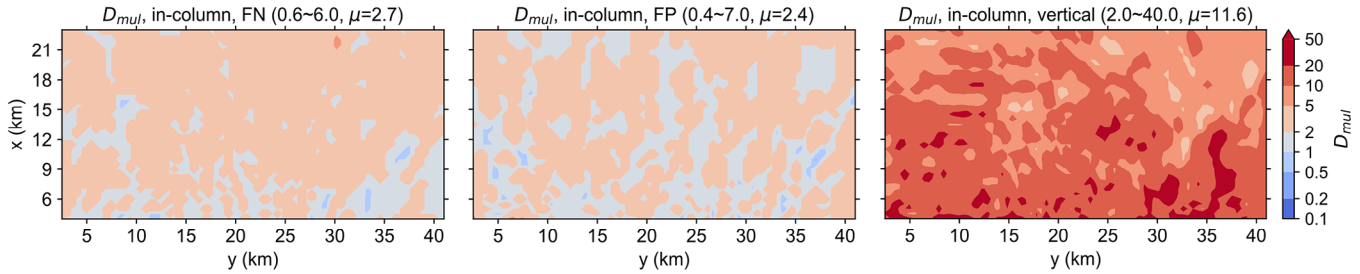

FIGURE 24 D_{mul} optimized for 1D SRA with in-column input motions in the FN, FP and vertical directions for case 1. Note D_{mul} for each site is chosen to achieve a best fit of the spectral accelerations (within 0.2~0.5 s) between the 1D SRA prediction and the reference 3D SW4 solution. The values in the parenthesis for each subplot are the minimum, maximum, and median of the damping multipliers, respectively.

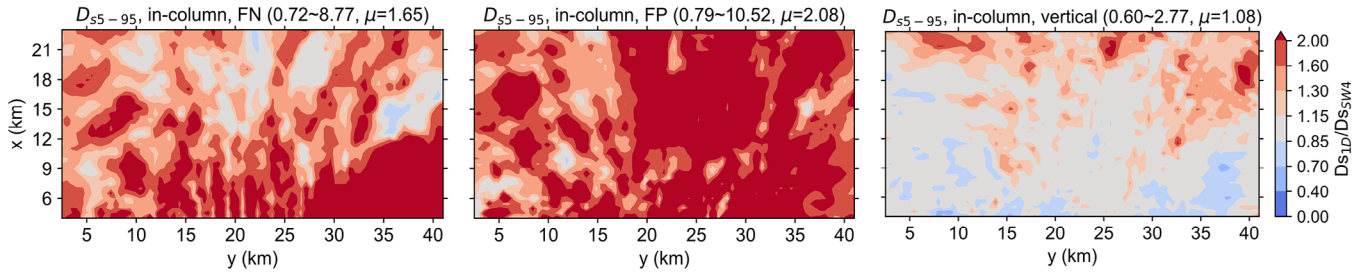

FIGURE 25 $Ds_{5\text{-}95}$ ratios of the 1D SRA predictions with in-column input motion to the reference 3D SW4 solution (case 1) for surface motions in the FN, FP and vertical directions. The values in the parenthesis for each subplot are the minimum, maximum and median of the ratios, respectively.

To examine the site dependency of D_{mul}, the damping multipliers optimized for the FN, FP and vertical directions at all sites in the domain are shown in Figure 24. As expected, since the optimization process for D_{mul} is driven by the SA ratios in the short-period range, the spatial variability of D_{mul} is in good correlation with the variation of short-period SA ratios with distance to the fault (Figure 19), that is, larger D_{mul} for the horizontal direction at the far-field sites due to increased P wave contribution, and larger D_{mul} for the vertical direction at the near-field sites due to the more significant constructive wave interference of P and S waves that contributes more to the high frequencies. It is noted that the D_{mul} needed for the best match scenario of the vertical component is generally much larger than that for the horizontal components due to the significant over-prediction of the vertical motion by the 1D approach. For the ground motion dataset simulated for case 1, the median D_{mul} optimized for the horizontal component is 2.7 and 2.4 for the FN and FP directions, respectively, and 11.6 for the vertical direction. Referring to the damping profile as shown in Figure 6E, these result lead to S and P wave damping ratios at the surface to be about 8% and 18% for the horizontal and vertical directions, respectively, consistent with the values used in previous site response studies for the horizontal and vertical motions[15,19] despite having been developed based on different methods of analysis. For instance, Tao and Rathje[15] recommend $D_{\text{mul}} = 3$ to account for additional sources of energy dissipation beyond material damping for the horizontal site response, while Elgamal and He[19] found very high viscous damping in the range of 15%−25% is needed to match the recorded vertical motions. These results indicate that the trapped waves in the soil column incurred by the 1D idealization procedure may have been a significant contributor to the frequent need of increased damping in the calibration of field site response studies.

Using the optimized D_{mul} for all the sites, Figure 25 shows the corresponding significant duration ratios of optimized 1D predictions to the reference 3D motions from SW4. Compared to the significant duration ratios computed with the original damping profile (Figure 18), the 1D predictions using the optimized damping are greatly improved. The observed strong spatial correlation between Figures 24 and 25, that is, larger D_{mul} leads to shorter significant duration, demonstrates the effectiveness of increased damping in removing the trapped energy in the 1D column. It is interesting to note that although the SA of horizontal and vertical motions are optimized close to the same level of agreement between the reference 3D solutions and 1D predictions as shown in Figure 22, the $Ds_{5\text{-}95}$ ratio maps after optimization show significantly better improvement in the vertical component, indicating the strong influence of trapped waves in the 1D vertical motion predictions when using the in-column input motion.

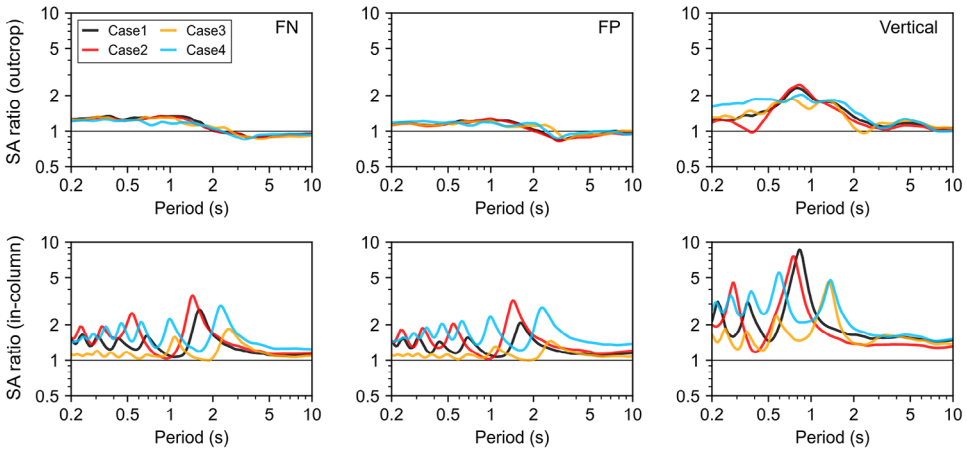

FIGURE 26 Median surface motion SA ratios of the 1D SRA predictions to the reference 3D SW4 solutions for the four basin profile cases in the FN (left column), FP (middle column) and vertical (right column) directions when using outcrop input motions (top row) and in-column input motions (bottom row).

5.4 | Effect of sedimentary basin profile on the accuracy of the 1D modelling approach

Apart from the within-event spatial variability demonstrated in the previous section, the accuracy of the 1D predictions is also expected to vary between different basin geologic profiles as a corollary of the physical nature of the inclined wave refraction and 1D wave trapping mechanisms. For shallow sedimentary basins considered in this study, the 3D ground motions will be determined by the earthquake source and basin geologic structure. Since we are primarily interested in providing physical understanding of the implications of approximating 3D wavefields with the simplified 1D approach, in this section we have considered four different sedimentary basin profiles as shown in Figure 6 while maintaining the same kinematic rupture model such that the effect of different basin properties, including the velocity gradient, impedance contrast at the rock-basin interface and basin depth, can be investigated under the same incident wavefield. As for the baseline case 1, we performed 1D SRA to approximate the 3D wavefields from SW4 simulations for basin profile cases 2∼4.

Figure 26 shows the comparison of median SA ratios of the 1D SRA predictions to the 3D reference motions for the four cases. On the whole, the four basin profile cases have demonstrated similar prediction bias in the horizontal and vertical directions. Except the under-prediction at long periods (> 2 s) when using the outcrop input motion, the SA ratios of the 1D predictions to the reference 3D solutions indicate overall over-prediction of both the horizontal and vertical surface motions by the simplified 1D approach due to the contribution of inclined P and S waves to the horizontal and vertical input motions for 1D SRA, respectively. As illustrated earlier, since the incident wavefield is controlled by the large-amplitude S waves and remains the same for the four cases, 1D SRA shows two levels of accuracy for the horizontal and vertical motion estimations, with the surface motion over-prediction being most prominent in the vertical direction. The SA ratios calculated based on the in-column input motion are characterized by the large amplification near the site periods in both the horizontal and vertical directions and the SA ratios show consistent shift in the site vibration periods, while it is noted that the over-prediction bias using the outcrop motion remained relatively stable due to the much less significant wave trapping phenomenon. Consistent variation of the SA ratios between the four cases is observed, as expected, and a detailed examination shows that this is caused by the discrepancies in the 3D wavefield composition due to the respective change of basin properties compared to the baseline case 1, as discussed further below.

5.4.1 | Velocity gradient

In consideration of the dominant S waves in the 3D wavefield, velocity gradient in the basin affects the wavefield composition in mainly two aspects: (1) the refraction process of inclined S waves, and (2) the efficiency of S-to-P wave conversion. With reduced basin velocity gradient in case 2 compared to case 1, S waves with larger wave speed undergo less refraction when propagating through the basin profile and the S-to-P wave conversion is less efficient. The reference surface

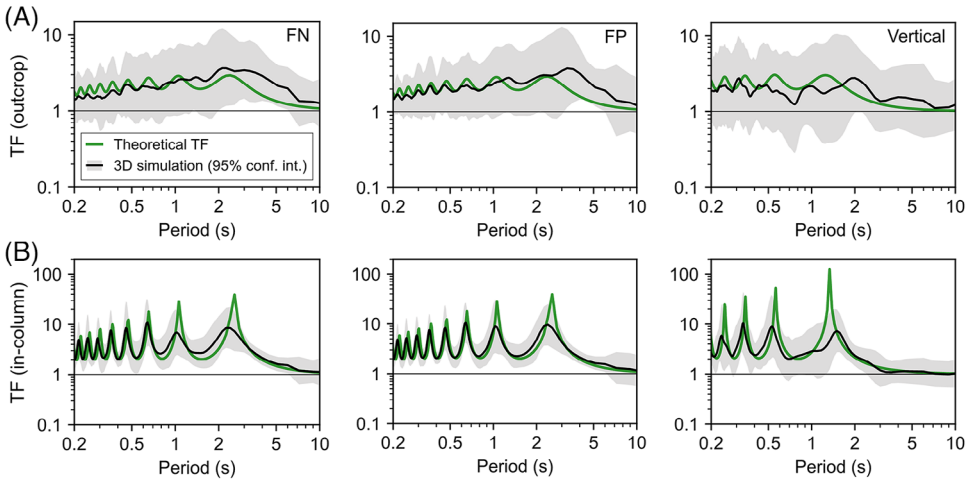

FIGURE 27 Comparison of the theoretical and 3D simulated TFs of case 3 calculated in the FN, FP and vertical directions when assuming: (A) outcrop boundary condition; (B) in-column boundary condition. The black line and the grey area represent the median ±2 standard deviations (i.e., 95% confidence interval).

motions in the 3D site response are more dominated by direct inclined S waves that are less refracted compared to the 1D input motions. As seen in Figure 26, for the horizontal motions, due to the greater travel time difference between the more inclined 3D waves and the idealized 1D waves and the less efficient attenuation for seismic waves with longer wavelengths, more significant wave trapping in the 1D soil column as evidenced by the larger SA amplification peaks is observed when using the in-column input motion. In the vertical direction, the less pronounced S wave refraction process has resulted in overall reduced over-prediction of the vertical motion with both the outcrop and in-column input motions. Since the outcrop input motions are the same for case 1 and case 2, the slight increase of SA ratio near the vertical fundamental site period (0.75 s) when using the outcrop inputs is caused by the less contribution of S-converted P waves in the 3D wavefield that leads to decreased 3D vertical site response at this period. Conversely, it is noted that the simplified 1D approach is also not able to capture the large amplification near period 0.4 s in the 3D site response, leading to the trough in the SA ratio at this period.

5.4.2 | Impedance contrast

In Figure 26, the SA ratios computed for case 3 with a rock to soil impedance contrast of about 1.56 at the rock-basin interface have shown substantial improvement in the 1D modelling accuracy in both the horizontal and vertical directions compared to case 1, especially when using the in-column input motion. The better agreement between the reference 3D solutions and 1D predictions is also observed in the comparison of the theoretical TFs assuming 1D wave propagation and the 3D simulated TFs computed using the reference 3D motions, as shown in Figure 27. Compared to the TFs for case 1 (Figure 13), the 3D-1D comparison is significantly improved in terms of both the alignment of resonance frequencies and the transfer function amplitude.

The above observations are explained by examining the change in the wavefield composition of the horizontal and vertical motions due to the employed velocity discontinuity in case 3. It is well-known that at soil layer interfaces, seismic waves are reflected and transmitted due to the impedance contrast between the adjacent layers. For the dominant S waves in the 3D wavefield, the large impedance contrast at the basin-rock interface has led to efficient S-to-P wave conversion and wave refraction towards the vertical direction, resulting in more significant contribution of direct S waves to the horizontal motion and S-converted P waves to the vertical motion, respectively. The horizontal and vertical site amplification process is therefore less coupled and better aligned with the 1D assumption, leading to improved 1D predictions for both the horizontal and vertical components.

To investigate the sensitivity of the wavefield composition on the impedance contrast and corresponding implications for the 1D approximation, for demonstration purposes, we consider a generic two-layered soil-rock system with rock to soil impedance contrast $\gamma = \rho_r v_r / \rho_s v_s$ (ρ and v are the density and wave speed, respectively), as shown in Figure 28A. For a dominant upgoing incident SV plane wave from the half-space, four resulting plane waves are generated to satisfy

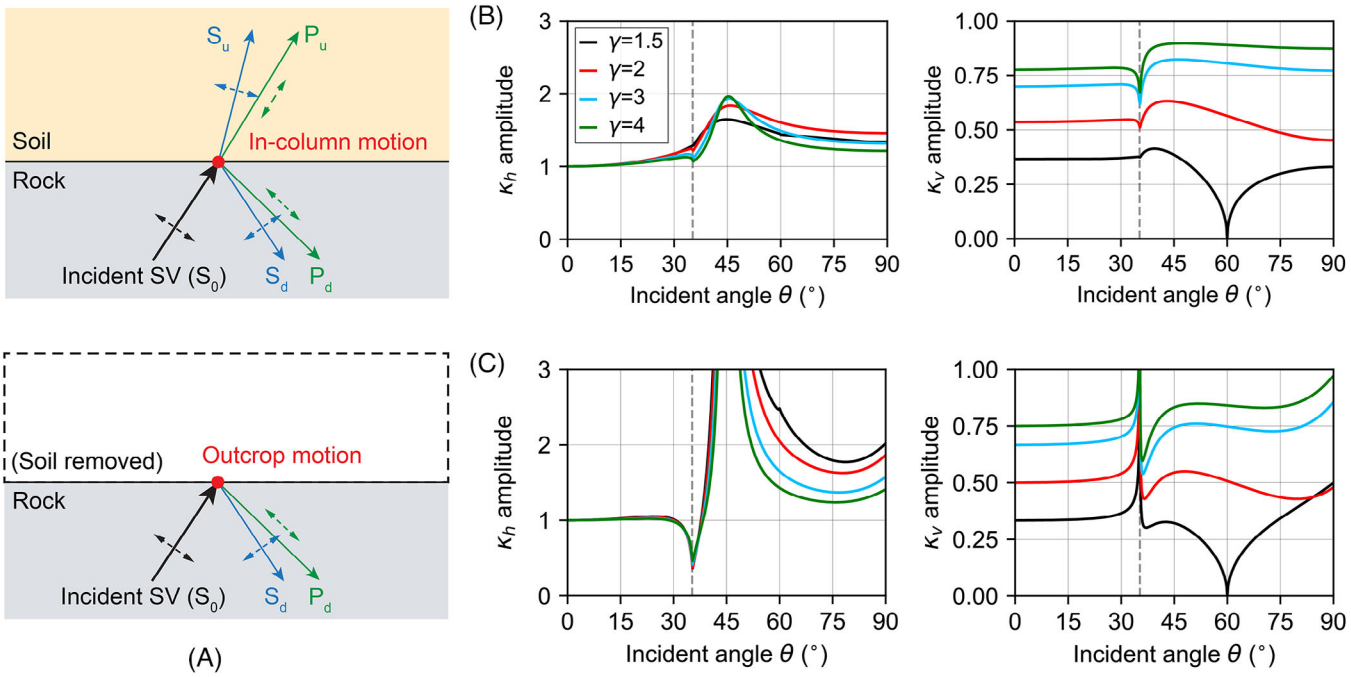

FIGURE 28 Wave contribution to the horizontal and vertical motions in the soil for a two-layered soil-rock system (Poisson's ratio $\nu = 0.25$) for different impedance contrast γ: (A) reflected and transmitted waves at the rock-soil interface due to inclined incident SV wave with amplitude S_0; (B) κ_h and κ_v when using the in-column input motion; (C) κ_h and κ_v when using the outcrop input motion. Vertical dashed lines in (B) and (C) represent the critical angle θ_{cr} of the incident SV wave.

the requirement for continuity of displacements and stresses at the interface, namely, the downgoing reflected SV and P waves in the half-space, and the upgoing transmitted SV and P waves in the soil layer. For quantifying the theoretical contribution of S waves to the horizonal surface motion and P waves to the vertical surface motion, we calculate the amplitude ratio of the transmitted SV wave to the total horizontal motion κ_h at the interface, and the transmitted P wave to the total vertical motion κ_v at the interface, respectively, based on the elastic reflection and transmission coefficients available in the literature,[67] that is,

$$\bullet \text{ For in} - \text{column input motion}: \quad \kappa_h = \frac{S_u^h}{P_u^h + S_u^h}, \kappa_v = \frac{P_u^v}{P_u^v + S_u^v} \tag{3}$$

$$\bullet \text{ For outcrop input motion}: \quad \kappa_h = \frac{S_u^h}{\frac{1}{2}\left(S_0^h + S_d^h + P_d^h\right) A_t}, \kappa_v = \frac{P_u^v}{\frac{1}{2}\left(S_0^v + S_d^v + P_d^v\right) A_t} \tag{4}$$

where S_0, S_u, P_u, S_d and P_d are the amplitudes of the incident SV, upgoing SV and P, and downgoing SV and P waves, respectively, with the superscripts h and v denoting the horizontal and vertical components, respectively; A_t is the transmission coefficient for 1D waves from rock to soil and is defined by $A_t = 2/(1 + 1/\gamma)$. Note that when using outcrop input motions, the total horizontal and vertical motion at the interface in Equation (4) are calculated based on a complementary rock outcrop model where the soil layer is removed. For the two-layered system, κ_h and κ_v are dependent on the interlayer impedance ratio γ and the incident angle θ of the incoming SV wave. The two contribution factors are plotted in Figure 28B,C for $\gamma \sim (1.5, 4)$ and $\theta \sim (0, 90)$, with the critical incident angle θ_{cr} denoted by the vertical dashed lines. It is observed that κ_h is close to 1 for $\theta < \theta_{cr}$ and becomes largely greater than 1 for $\theta > \theta_{cr}$, indicating the reasonable accuracy and potential under-prediction bias of the horizontal motion by 1D SRA at small and large incident angles, respectively. For the vertical motion, however, κ_v remains smaller than 1 across the entire incident angle range, implying the consistent over-prediction bias of the 1D approach when approximating wavefields dominated by inclined SV waves. A striking property of κ_h and κ_v in Figure 28B,C is that for θ smaller than θ_{cr}, which is true for practically observed angles of incidence in the field due to the upper crustal velocity gradients,[34] the two theoretical contribution factors demonstrate weak dependency on the incident angle θ, which is of special interest to the vertical motion estimation. Considering that the vertical site response is becoming dominated by the transmitted P wave with increasing impedance contrast (e.g., $\kappa_v > 0.5$ for γ

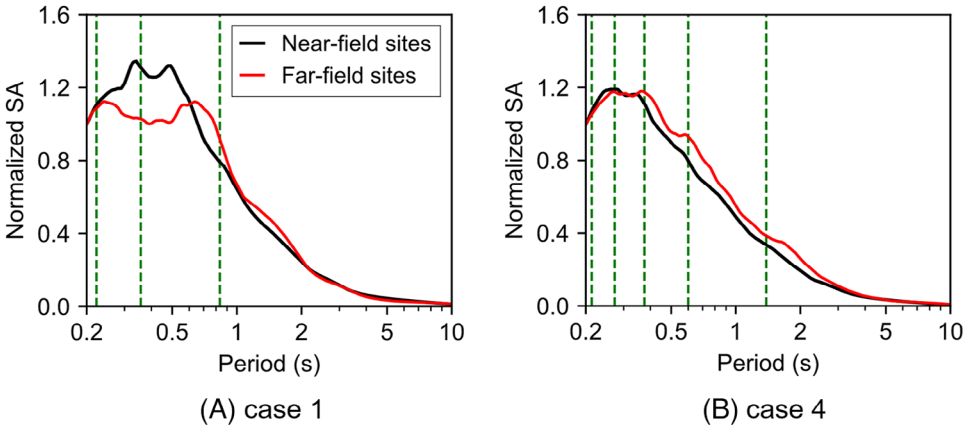

FIGURE 29 Normalized median SA (with respect to SA at 0.2 s) of the vertical outcrop input motions for sites in (A) case 1 and (B) case 4. The vertical dashed green lines show the site periods of the respective basin soil profile assuming a 1D vertical P wave propagation model.

larger than about 2), κ_v may serve as a theoretical upper-bound reduction factor for the over-predicted vertical motions by 1D SRA when applied to sites with large impedance contrasts, for example, in the central and eastern United States, provided that proper damping is chosen at the same time to damp out the trapped outgoing waves in the 1D soil column.

5.4.3 | Basin depth

Past earthquakes have shown that site amplification in deep sedimentary basins such as in the Southern California area and the Mexico City, can be detrimental to civil infrastructures. In case 4, the depth of the sedimentary layers is doubled to examine the effects of basin depth on the prediction bias of the 1D approach. In deeper soil deposits, the inclined shear waves emitted from the earthquake source impinge on the base of the basin at larger incident angles and are subjected to more significant wave refraction process before reaching the surface. As shown in Figure 26, this has exacerbated the extent of over-prediction of the vertical motion over a broader range of spectral periods and led to more wave trapping in the 1D soil column in both directions when using the in-column input motion. It is interesting to note that the increase in the median SA ratio compared to case 1 concentrates mostly in the short-period range, indicating more considerable overprediction in the high frequency components. To better interpret this result, we plot in Figure 29 the normalized SA of the vertical outcrop input motions for sites in case 1 and case 4. Note that similar observation can be made with the in-column input motions although the SA is influenced by the downgoing wave effect. It is seen that the vertical outcrop input motions for case 4 are richer in the high frequencies due to shorter wave travel paths of the inclined seismic waves while in case 1 the input motions show more broadband spectral response over the first three vibrate modes of the site, especially at large distances. Since the relative modal contribution to the site response is dependent on the match between the frequency contents of the excitation source and the vibration properties of the system, this explains the shift of period range where large amplifications occur towards higher site vibration modes in the deeper basin case.

6 | CONCLUSION

As one of the essential tasks in geotechnical earthquake engineering and engineering seismology, evaluation of local site effects is predominantly performed using 1D SRA due to its simplicity in concept and computational efficiency. However, since this 1D modelling approach only accounts for part of the physics that governs the site response, its accuracy is expected to vary when indiscriminately applied to engineering sites under different geological and tectonic settings. In view of the large uncertainties involved in the subsurface characterization and input motion selection for real-world sites, in this study, we evaluate the applicability of 1D SRA numerically based on spatially dense high-fidelity ground motions from well-controlled physics-based earthquake simulations resolved to a maximum frequency of 5 Hz. 3D seismic wave propagation in canonical shallow sedimentary basins is considered to obtain the reference 3D site response solutions and the input motions for 1D SRA at a total of 3159 effective downhole array sites in the computational domain. The evaluation

is conducted through detailed site-to-site comparison of the reference true 3D site response solution and the corresponding 1D SRA predictions in terms of various frequency- and time-domain quantities. We examined the manifestation of the two deficiencies in 1D SRA previously identified based on idealized 2D plane waves and point earthquake source simulations, and discussed the discrepancies between the amplification mechanism of the 3D horizontal and vertical site response and that assumed in 1D SRA. The implications of the 1D approximation to 3D seismic wavefields were further illustrated in terms of the spatial variability of the 3D-1D comparisons and sensitivity studies on the basin damping and velocity profiles.

The more detailed analyses performed here confirm the two previously identified mechanistic limitations in the 1D modelling approach, that is, the systematic over-prediction of the vertical motion and wave trapping in the 1D soil column that leads to fictitiously long-duration motion. The vertical motion over-prediction by 1D SRA is caused by a combined effect of its inability to capture the shear wave refraction process and simultaneous amplification of the input motions through the classical 1D site amplification mechanism. The wave trapping is due to the travel path difference between the actual inclined waves and the assumed 1D waves that leads to trapped outgoing waves and spurious resonance in the soil column. Different levels of accuracy of 1D SRA for the horizontal and vertical motion estimation, as observed in previous field investigations, have been recognized. The root cause is the discrepancies between the actual 3D amplification mechanism of coupled horizontal and vertical site response and the simplified uncoupled 1D site amplification assumed in 1D SRA. For shallow sedimentary basins, inclined S waves dominate the horizontal motions, and they either dominate or contribute significantly to the vertical component. Although the accuracy of 1D predictions for both the horizontal and vertical motions are complicated by the trapped waves when using the in-column input, this phenomenon is more pronounced for the vertical motion due to the over-prediction of this component and differences in the wave speed and attenuation rate. Due to the upper crustal velocity gradient and finite dimension of the computational domain, the incident angle of S waves remains relatively small when arriving at the rock-basin interface, the underprediction of the horizontal motion as would be expected when approximating inclined S waves propagating at large incident angles is not broadly observed using the simulated ground motion datasets in this study.

The accuracy of the simplified 1D approach has shown significant spatial variability in the computational domain due to the spatial and temporal evolution of the wavefield composition of the 1D input motions. Through numerical simulations of a baseline earthquake scenario with two levels of crustal P wave damping – the original small P wave damping and the modified large P wave damping (10%), it is demonstrated that with increasing distance to the fault: (1) the relative P wave contribution to both the outcrop and in-column input motions increases due to the lower wave attenuation of P waves compared to S waves, (2) the time separation between the P and S wave windows increases due to the velocity difference between P and S waves, (3) the dominant frequencies in the S waves are shifted towards lower frequencies as the high frequencies are attenuated. Due to the increased P wave contribution to the horizontal input motions with increasing source-to-site distance, the horizontal surface motions are over-predicted by 1D SRA due to its inability to model the gradual refraction of inclined P waves. Since the vertical motion over-prediction is driven by the significant contribution of S waves in the input motions, the time separation between the P and S wave windows leads to less constructive interferences between the two wave types in the high-frequency range and shift of the resonant frequencies towards lower modal frequencies of the site.

In existing site response studies, due to lack of measured attenuation properties, the soil damping profile is often empirically increased to improve the agreement between the 1D SRA predictions and the field recordings. To investigate the characteristics of the trapped waves incurred by the 1D approximation and the efficacy of increased soil damping in the improvement of the 1D SRA results with the in-column input motions, we followed a similar approach where we scale the reference soil damping profile used in the 3D SW4 simulations by a damping multiplier D_{mul} to achieve a best fit of SA within the short-period range 0.2~0.5 s between the 1D predictions and reference 3D solutions. The results show D_{mul} values that are compatible with those found in the literature for both horizontal and vertical motions. Compared to the horizontal motions, a larger D_{mul} is typically required for the vertical motion prediction due to the significant over-prediction of this component by the 1D approach. The efficacy of increased soil profile damping varies across the sites and is dependent on the spatial and temporal evolution of the incident wavefield. Due to the increased P wave contribution to the horizontal input motions with increasing source-to-site distance, D_{mul} optimized for the horizontal motions is larger for the far-field sites compared to the near-field sites. Conversely, as the vertical motion over-prediction is driven by the significant contribution of S waves in the input motions, the time separation between the P and S wave windows leads to less constructive interferences between the two wave types in the high-frequency range and results in smaller D_{mul} required for the sites in the far-field. Since wave scattering is not the underlying cause of the trapped waves, increasing the damping to improve the 1D site response predictions can only be performed on a site-to-site basis.

Apart from the within-event spatial variability, sensitivity study on the properties of the basin geologic profile, including the velocity gradient, rock-basin impedance contrast and basin depth further demonstrates the dependency of the performance of the 1D approach on the characteristics of the true 3D site response to which the 1D method is to approximate. By and large, the sensitivity results confirm the general observations made in our baseline case 1, for example, overall over-prediction of the surface motions and higher levels of amplification near the site periods by 1D SRA, both occurring more prominently in the vertical direction. It is observed that decreasing the velocity gradient of the basin profile leads to less refraction of the dominant S waves and overall reduction in the vertical motion over-prediction bias, while the horizontal motion estimations suffer from more significant wave trapping phenomena when approximating inclined S waves with larger incident angles. Increasing the basin depth leads to higher vertical 1D amplification in the short-period range due to the change in the frequency contents of the input motions, and more broadband over-prediction of the surface motions when using the in-column motions due to wave trapping. Among the three basin profile properties, it is found that the impedance contrast at the rock-basin interface has the most significant impact on the modelling bias. Compared to case 1 where there is no impedance mismatch at the interface, the large velocity contrast at the bottom of the sedimentary basin in case 3 leads to efficient S-to-P wave conversion. As a result, the horizontal and vertical motions are less coupled and are more dominated by the upgoing S and P waves, respectively, in better alignment with the 1D assumption, and therefore the accuracy of 1D predictions are substantially improved.

The results of this study suggest that for shallow sedimentary basins, the horizontal motions can be reasonably approximated by a 1D S wave propagation model to the first order, while the 1D P wave propagation model for vertical motions misrepresents the propagation physics of inclined S waves and leads to consistent over-prediction bias. For the shallow basins study performed here, 1D SRA for vertical motion estimation is not reliable and should only be considered for velocity profiles with large impedance contrast at the base such that the assumption of P waves governing the vertical site response is justified. Given that the relative contribution of refracted S and P waves to the total wavefield in the soil layer after S-to-P wave conversion is not significantly sensitive to modest changes in the angle of incidence in the small to intermediate range typical under most field conditions, this property may be useful in developing empirical correction factors for the 1D vertical motion prediction. To mitigate the spurious resonance introduced in the 1D idealization of inclined seismic waves, the utilization of increased levels of damping, as empirically calibrated in past site response studies, may be one option in practical engineering applications. For the simulated ground motion datasets used in this study, we found the median damping multiplier D_{mul} for the horizontal and vertical components of motion in the ranges of 1.5∼3 and 4∼15, respectively, resulting in damping ratios at the surface about 4.5%∼9% for the S waves and 6%∼22% for the P waves, consistent with observations in past field studies.[15,19,26] More detailed ground shaking modelling based on 2D inclined plane waves[32,38] or fully 3D solutions, which can rigorously represent the mechanics of inclined incident waves, can contribute to the ultimate solution for improving the predictions of both the horizontal and vertical motions, especially in forensic site response studies[11] where the earthquake source and soil profile are better characterized.

Although in this study we evaluated the accuracy of 1D SRA and the implications when applying this 1D modelling approach to realistic 3D seismic wavefields, it is important to note that our assessments were based on simulated 3D site response in the simple canonical basin models, which may not capture all the complexities that contribute to real-world site response and alternative geophysical conditions. For instance, narrow and deep sedimentary valleys may exhibit whole basin resonance patterns and generate seismic wavefields that can differ from that in shallow sedimentary basins, which may explain the underprediction by the 1D approach found in selected past studies. In addition, irregular topography, soil nonlinearity and lateral heterogeneity will further complicate the determination of the range of applicability of the 1D approach. The investigation of these contributing factors is, however, beyond the scope of this paper and left to future research. Understanding on an a priori basis the full spectrum of situations where 1D SRA may not be effective remains an unsolved challenge, and the findings in this study will work towards the long-term goal of incorporating more adequate physics into this problem to improve the overall site response prediction for engineering applications.

ACKNOWLEDGEMENTS

The authors would like to thank Dr. Arben Pitarka of Lawrence Livermore National Laboratory for providing the input on the Graves-Pitarka kinematic rupture model for the extended source earthquake representation. Computer access and exceptional support from the National Energy Research Scientific Computing Center (NERSC) at Lawrence Berkeley National Lab is gratefully acknowledged. This research was enabled by the software developments of the Exascale Computing Project (ECP), Project Number: 17-SC-20-SC, a collaborative effort of two U.S. Department of Energy organizations—the Office of Science and the National Nuclear Security Administration, simulation runs and analysis of results were supported by the U.S. Department of Energy Nuclear Safety Research and Development (NSRD) Program.

DATA AVAILABILITY STATEMENT

The authors will assemble the simulation data from this study and plan to submit to DesignSafe for community access.

ORCID

Junfei Huang https://orcid.org/0000-0001-6133-1004
David McCallen https://orcid.org/0000-0003-0386-0324

REFERENCES

1. Kanai K. The effect of solid viscosity of surface layer on the earthquake movements. *Bull Earthq Res Inst*. 1950;28(1):31-35.
2. Idriss IM, Seed HB. Seismic response of horizontal soil layers. *J Soil Mech Found Div*. 1968;94(4):1003-1031.
3. Schnabel P, Seed HB, Lysmer J. Modification of seismograph records for effects of local soil conditions. *Bull Seismol Soc Am*. 1972;62(6):1649-1664. doi:10.1785/BSSA0620061649
4. Kamai R, Abrahamson NA, Silva WJ. Nonlinear horizontal site amplification for constraining the NGA-West2 GMPEs. *Earthq Spectra*. 2014;30(3):1223-1240. doi:10.1193/070113EQS187M
5. Shi J, Asimaki D. From stiffness to strength: formulation and validation of a hybrid hyperbolic nonlinear soil model for site-response analyses. *Bull Seismol Soc Am*. 2017;107(3):1336-1355. doi:10.1785/0120150287
6. Ostadan F, Kennedy R. Consistent site-response/soil-structure interaction analysis and evaluation. *Nucl Eng Des*. 2014;269:72-77. doi:10.1016/j.nucengdes.2013.08.009
7. Stewart JP, Afshari K, Hashash YMA. *Guidelines for Performing Hazard-Consistent One-Dimensional Ground Response Analysis for Ground Motion Prediction*. Pacific Earthquake Engineering Research Center, University of California; 2014. PEER Report 2014/16.
8. Kaklamanos J, Cabas A, Parolai S, Guéguen P. Introduction to the special section on advances in site response estimation. *Bull Seismol Soc Am*. 2021;111(4):1665-1676. doi:10.1785/0120210152
9. Thompson EM, Baise LG, Tanaka Y, Kayen RE. A taxonomy of site response complexity. *Soil Dyn Earthq Eng*. 2012;41:32-43. doi:10.1016/j.soildyn.2012.04.005
10. Kaklamanos J, Bradley BA, Moolacattu AN, Picard BM. Physical hypotheses for adjusting coarse profiles and improving 1D site-response estimation assessed at 10 KiK-net sites. *Bull Seismol Soc Am*. 2020;110(3):1338-1358. doi:10.1785/0120190263
11. Ntritsos N, Cubrinovski M, Bradley BA. Challenges in the definition of input motions for forensic ground-response analysis in the near-source region. *Earthq Spectra*. 2021;37(4):2562-2595. doi:10.1177/87552930211001376
12. Boore DM. Can site response be predicted? *J Earthq Eng*. 2004;8(sup001):1-41. doi:10.1080/13632460409350520
13. Kaklamanos J, Bradley BA. Challenges in predicting seismic site response with 1D analyses: conclusions from 114 KiK-net vertical seismometer arrays. *Bull Seismol Soc Am*. 2018;108(5A):2816-2838. doi:10.1785/0120180062
14. Pilz M, Cotton F. Does the one-dimensional assumption hold for site response analysis? A study of seismic site responses and implication for ground motion assessment using KiK-Net strong-motion data. *Earthq Spectra*. 2019;35(2):883-905. doi:10.1193/050718EQS113M
15. Tao Y, Rathje E. Taxonomy for evaluating the site-specific applicability of one-dimensional ground response analysis. *Soil Dyn Earthq Eng*. 2020;128:105865. doi:10.1016/j.soildyn.2019.105865
16. Aoi S, Kunugi T, Fujiwara H. Trampoline effect in extreme ground motion. *Science*. 2008;322(5902):727-730. doi:10.1126/science.1163113
17. Bradley BA, Cubrinovski M. Near-source strong ground motions observed in the 22 February 2011 Christchurch Earthquake. *Seismol Res Lett*. 2011;82(6):853-865. doi:10.1785/gssrl.82.6.853
18. Papazoglou AJ, Elnashai AS. Analytical and field evidence of the damaging effect of vertical earthquake ground motion. *Earthq Eng Struct Dyn*. 1996;25(10):1109-1137. doi:10.1002/(SICI)1096-9845(199610)25:10⟨1109::AID-EQE604⟩3.0.CO;2-0
19. Elgamal A, He L. Vertical earthquake ground motion records: an overview. *J Earthq Eng*. 2004;8(5):663-697. doi:10.1080/13632460409350505
20. Newmark NM, Hall WJ. Development of Criteria for Seismic Review of Selected Nuclear Power Plants. 1978. NUREG/CR-0098. doi:10.2172/6704054
21. American Society of Civil Engineers. Minimum Design Loads and Associated Criteria for Buildings and Other Structures. American Society of Civil Engineers; 2017. doi:10.1061/9780784414248
22. Stewart JP, Boore DM, Seyhan E, Atkinson GM. NGA-West2 equations for predicting vertical-component PGA, PGV, and 5%-Damped PSA from shallow crystal earthquakes. *Earthq Spectra*. 2016;32(2):1005-1031. doi:10.1193/072114eqs116m
23. Ostadan F, Deng N. *Advanced Nuclear Technology: Modeling Vertical Free-Field Motion for Soil-Structure Interaction of Embedded Structures*. Electric Power Research Institute; 2018:3002011804.
24. American Society of Civil Engineers. *Seismic Design Criteria for Structures, Systems, and Components in Nuclear Facilities*. American Society of Civil Engineers; 2005.
25. Mok CM, Chang CY, Legaspi DE. Site response analyses of vertical excitation. *Geotechnical Earthquake Engineering and Soil Dynamics III*. American Society of Civil Engineers; 1998:739-753. Accessed November 18, 2023. https://cedb.asce.org/CEDBsearch/record.jsp?dockey=0112737
26. Tsai CC, Liu HW. Site response analysis of vertical ground motion in consideration of soil nonlinearity. *Soil Dyn Earthq Eng*. 2017;102:124-136. doi:10.1016/j.soildyn.2017.08.024

27. Abrahamson N, Pinilla-Ramos C, Tehrani P, Perez M, Krimotat A. Modeling of vertical component ground motion for soil-structure-interaction analyses. 26th International Conference on Structural Mechanics in Reactor Technology. International Association for Structural Mechanics in Reactor Technology; 2022:8.
28. Johnson LR, Silva W. The effects of unconsolidated sediments upon the ground motion during local earthquakes. *Bull Seismol Soc Am*. 1981;71(1):127-142. doi:10.1785/BSSA0710010127
29. Fujii N, Annaka T, Ohki H, Fujitani M, Yasuda N. A study on the characteristics of seismic vertical motion. Proceedings of the Tenth World Conference on Earthquake Engineering. Vol 10. International Association for Earthquake Engineering; 1992:577-582.
30. Yang J, Yan XR. Site response to vertical earthquake motion. Geotechnical Earthquake Engineering and Soil Dynamics IV. American Society of Civil Engineers; 2012:1-8. doi:10.1061/40975(318)23
31. Zhang W, Seylabi E, Taciroglu E. Effects of soil stratigraphy on dynamic soil-structure interaction behavior of large underground structures. Proceedings of the 3rd International Conference on Performance-Based Design in Earthquake Geotechnical Engineering. International Society for Soil Mechanics and Geotechnical Engineering; 2017.
32. Zhang W, Taciroglu E. 3D time-domain nonlinear analysis of soil-structure systems subjected to obliquely incident SV waves in layered soil media. *Earthq Eng Struct Dyn*. 2021;50(8):2156-2173. doi:10.1002/eqe.3443
33. Silva W. Characteristics of vertical strong ground motions for applications to engineering design. Proc. Of the FHWA/NCEER Workshop on the National Representation of Seismic Ground Motion for New and Existing Highway Facilities. Technical Rept. NCEER-97-0010; 1997:1-48.
34. Beresnev IA, Nightengale AM, Silva WJ. Properties of vertical ground motions. *Bull Seismol Soc Am*. 2002;92(8):3152-3164. doi:10.1785/0120020009
35. Takahashi K, Ohno S, Takemura M, Ohta T. Observation of earthquake strong motion with deep borehole—generation of vertical motion propagating in surface layers after S-wave arrival. Proceedings of the Tenth World Conference on Earthquake Engineering. Vol 3. International Association for Earthquake Engineering; 1992.
36. Bonilla LF, Steidl JH, Gariel JC, Archuleta RJ. Borehole response studies at the Garner Valley Downhole Array, Southern California. *Bull Seismol Soc Am*. 2002;92(8):3165-3179. doi:10.1785/0120010235
37. Chao SH, Kuo CH, Lin CM, Huang JY, Rathje E, Abrahamson N. Observed nonlinear site amplification of vertical ground motion in Taiwan. *Earthq Spectra*. 2023;39(4):2379-2405. doi:10.1177/87552930231190985
38. Huang J, McCallen D. Predicament of the 1D assumption in site response analysis and implications for vertical ground motion assessment. Proceedings of the 9th International Conference on Computational Methods in Structural Dynamics and Earthquake Engineering. European Community on Computational Methods in Applied Sciences; 2023:900-924. doi:10.7712/120123.10445.21275
39. McCallen D, Petersson A, Rodgers A, et al. EQSIM—a multidisciplinary framework for fault-to-structure earthquake simulations on exascale computers part I: computational models and workflow. *Earthq Spectra*. 2021;37(2):707-735. doi:10.1177/8755293020970982
40. Petrone F, Abrahamson N, McCallen D, Pitarka A, Rodgers A. Engineering evaluation of the EQSIM simulated ground-motion database: the San Francisco Bay Area Region. *Earthq Eng Struct Dyn*. 2021;50(15):3939-3961. doi:10.1002/eqe.3540
41. Matinrad P, Petrone F. ASCE/SEI 7-compliant site-specific evaluation of the seismic demand posed to reinforced concrete buildings with real and simulated ground motions. *Earthq Eng Struct Dyn*. 2023;52(15):4987-5009. doi:10.1002/eqe.3995
42. Rodgers AJ, Petersson A, Pitarka A, McCallen DB, Sjogreen B, Abrahamson N. Broadband (0–5 Hz) fully deterministic 3D ground-motion simulations of a magnitude 7.0 Hayward Fault earthquake: comparison with empirical ground-motion models and 3D path and site effects from source normalized intensities. *Seismol Res Lett*. 2019;90(3):1268-1284. doi:10.1785/0220180261
43. McCallen D, Tang H, Wu S, Eckert E, Huang J, Petersson NA. Coupling of regional geophysics and local soil-structure models in the EQSIM fault-to-structure earthquake simulation framework. *Int J High Perform Comput Appl*. 2022;36(1):78-92. doi:10.1177/10943420211019118
44. Kramer SL. *Geotechnical Earthquake Engineering*. Prentice-Hall; 1996.
45. Boore DM. The uses and limitations of the square-root-impedance method for computing site amplification. *Bull Seismol Soc Am*. 2013;103(4):2356-2368. doi:10.1785/0120120283
46. Tao Y, Rathje E. Insights into modeling small-strain site response derived from downhole array data. *J Geotech Geoenvironmental Eng*. 2019;145(7):04019023. doi:10.1061/(ASCE)GT.1943-5606.0002048
47. Pretell R, Abrahamson NA, Ziotopoulou K. A borehole array data–based approach for conducting 1D site response analyses I: damping and VS randomization. *Earthq Spectra*. 2023;39(3):1473-1501. doi:10.1177/87552930231173445
48. Petersson N, Sjogreen B. User's Guide to SW4, Version 2.0. Lawrence Livermore National Laboratory; 2017. LLNL-SM-741439.
49. McCallen D, Petrone F, Miah M, Pitarka A, Rodgers A, Abrahamson N. EQSIM—a multidisciplinary framework for fault-to-structure earthquake simulations on exascale computers, Part II: regional simulations of building response. *Earthq Spectra*. 2021;37(2):736. doi:10.1177/8755293020970980
50. National Energy Research Scientific Computing Center. Perlmutter. NERSC Documentation. Accessed April 29, 2024. https://docs.nersc.gov/systems/perlmutter/
51. Graves R, Pitarka A. Kinematic ground-motion simulations on rough faults including effects of 3D stochastic velocity perturbations. *Bull Seismol Soc Am*. 2016;106(5):2136-2153. doi:10.1785/0120160088
52. Pitarka A, Graves R, Irikura K, et al. Refinements to the Graves–Pitarka Kinematic Rupture Generator, including a dynamically consistent slip-rate function, applied to the 2019 Mw 7.1 Ridgecrest earthquake. *Bull Seismol Soc Am*. 2021;112(1):287-306. doi:10.1785/0120210138

53. Mylonakis GE, Rovithis E, Parashakis H. 1D Seismic response of soil: continuously inhomogeneous vs equivalent homogeneous soil. Proceedings of the 3rd International Conference on Computational Methods in Structural Dynamics and Earthquake Engineering. European Community on Computational Methods in Applied Sciences; 2011.
54. Campbell KW. Estimates of shear-wave Q and $\kappa 0$ for unconsolidated and semiconsolidated sediments in Eastern North America. *Bull Seismol Soc Am*. 2009;99(4):2365-2392. doi:10.1785/0120080116
55. Afshari K, Stewart JP. *Effectiveness of 1D Ground Response Analyses at Predicting Site Response at California Vertical Array Sites*. University of California; 2022. https://escholarship.org/uc/item/4qd93847
56. Taborda R, Roten D. Physics-based ground-motion simulation. *Encyclopedia of Earthquake Engineering*. Springer-Verlag; 2015:1-33. doi:10.1007/978-3-642-36197-5_240-1
57. Petrone F, Abrahamson N, McCallen D, Miah M. Validation of (not-historical) large-event near-fault ground-motion simulations for use in civil engineering applications. *Earthq Eng Struct Dyn*. 2021;50(1):116-134. doi:10.1002/eqe.3366
58. Boore DM. Orientation-independent, nongeometric-mean measures of seismic intensity from two horizontal components of motion. *Bull Seismol Soc Am*. 2010;100(4):1830-1835. doi:10.1785/0120090400
59. Abrahamson NA, Silva WJ, Kamai R. Summary of the ASK14 ground motion relation for active crustal regions. *Earthq Spectra*. 2014;30(3):1025-1055. doi:10.1193/070913EQS198M
60. Gülerce Z, Kamai R, Abrahamson NA, Silva WJ. Ground motion prediction equations for the vertical ground motion component based on the NGA-W2 Database. *Earthq Spectra*. 2017;33(2):499-528. doi:10.1193/121814EQS213M
61. Boore DM, Stewart JP, Seyhan E, Atkinson GM. NGA-West2 equations for predicting PGA, PGV, and 5% damped PSA for shallow crustal earthquakes. *Earthq Spectra*. 2014;30(3):1057-1085. doi:10.1193/070113EQS184M
62. Campbell KW, Bozorgnia Y. NGA-West2 ground motion model for the average horizontal components of PGA, PGV, and 5% damped linear acceleration response spectra. *Earthq Spectra*. 2014;30(3):1087-1115. doi:10.1193/062913EQS175M
63. Bozorgnia Y, Campbell KW. Vertical ground motion model for PGA, PGV, and linear response spectra using the NGA-West2 database. *Earthq Spectra*. 2016;32(2):979-1004. doi:10.1193/072814eqs121m
64. Kawase H. The cause of the damage belt in Kobe: "The Basin-Edge Effect," constructive interference of the direct S-Wave with the basin-induced diffracted/Rayleigh waves. *Seismol Res Lett*. 1996;67(5):25-34. doi:10.1785/gssrl.67.5.25
65. Zalachoris G, Rathje EM. Evaluation of one-dimensional site response techniques using borehole arrays. *J Geotech Geoenvironmental Eng*. 2015;141(12):04015053. doi:10.1061/(ASCE)GT.1943-5606.0001366
66. Baker J, Bradley B, Stafford P. *Seismic Hazard and Risk Analysis*. Cambridge University Press; 2021. https://www.cambridge.org/core/books/seismic-hazard-and-risk-analysis/177B4BA01FC2600AA53A22B27598A06C
67. Aki K, Richards PG. *Quantitative Seismology*. 2nd ed. University Science Books; 2009.
68. Wolf JP. *Dynamic soil-Structure Interaction*. Prentice-Hall; 1985.
69. Steidl JH, Tumarkin AG, Archuleta RJ. What is a reference site? *Bull Seismol Soc Am*. 1996;86(6):1733-1748. doi:10.1785/BSSA0860061733

SUPPORTING INFORMATION

Additional supporting information can be found online in the Supporting Information section at the end of this article.

How to cite this article: Huang J, McCallen D. Applicability of 1D site response analysis to shallow sedimentary basins: A critical evaluation through physics-based 3D ground motion simulations. *Earthquake Engng Struct Dyn*. 2024;53:2876–2907. https://doi.org/10.1002/eqe.4142